

Neuronal activity in the isolated mouse spinal cord during spontaneous deletions in fictive locomotion: insights into locomotor central pattern generator organization

Guisheng Zhong¹, Natalia A. Shevtsova², Ilya A. Rybak² and Ronald M. Harris-Warrick¹

¹Department of Neurobiology and Behavior, Cornell University, Ithaca, NY, USA

²Department of Neurobiology and Anatomy, Drexel University College of Medicine, Philadelphia, PA, USA

Key points

- The organization of the spinal circuitry responsible for the generation of locomotor rhythm and control of locomotion in mammals is largely unknown, though several types of spinal interneurons involved in the rodent locomotor network have been identified.
- Ventral root recordings of spinal motoneurons during fictive locomotion in the isolated mouse spinal cord show spontaneous deletions of activity. The majority of deletions in the isolated neonatal mouse spinal cord are non-resetting: they do not change the phase of subsequent motor cycles. Flexor and extensor motoneurons express asymmetric responses during deletions: flexor deletions are accompanied by tonic ipsilateral extensor activity, while extensor deletions do not perturb rhythmic ipsilateral flexor activity. Non-resetting deletions on one side of the cord do not perturb rhythmic activity on the other side of the cord and can occur in isolated hemicords.
- We have characterized the activity of motoneurons and identified interneurons during spontaneous motor deletions. The motoneurons and a subset of V2a interneurons fall silent during non-resetting motor deletions while a second subset of V2a interneurons and commissural interneurons continue unperturbed rhythmic firing. This allowed us to suggest their involvement at different levels of the locomotor network operation.
- We have developed a computational model of the central pattern generator that reproduces, and proposes a mechanistic explanation for, our experimental results. The model provides novel insights into the organization of spinal locomotor networks.

Abstract We explored the organization of the spinal central pattern generator (CPG) for locomotion by analysing the activity of spinal interneurons and motoneurons during spontaneous deletions occurring during fictive locomotion in the isolated neonatal mouse spinal cord, following earlier work on locomotor deletions in the cat. In the isolated mouse spinal cord, most spontaneous deletions were non-resetting, with rhythmic activity resuming after an integer number of cycles. Flexor and extensor deletions showed marked asymmetry: flexor deletions were accompanied by sustained ipsilateral extensor activity, whereas rhythmic flexor bursting was not perturbed during extensor deletions. Rhythmic activity on one side of the cord was not perturbed during non-resetting spontaneous deletions on the other side, and these deletions could occur with no input from the other side of the cord. These results suggest that the locomotor CPG has a two-level organization with rhythm-generating (RG) and pattern-forming (PF) networks, in which only the flexor RG network is intrinsically rhythmic. To further explore the neuronal organization of the CPG, we monitored activity of motoneurons and selected identified

interneurons during spontaneous non-resetting deletions. Motoneurons lost rhythmic synaptic drive during ipsilateral deletions. Flexor-related commissural interneurons continued to fire rhythmically during non-resetting ipsilateral flexor deletions. Deletion analysis revealed two classes of rhythmic V2a interneurons. Type I V2a interneurons retained rhythmic synaptic drive and firing during ipsilateral motor deletions, while type II V2a interneurons lost rhythmic synaptic input and fell silent during deletions. This suggests that the type I neurons are components of the RG, whereas the type II neurons are components of the PF network. We propose a computational model of the spinal locomotor CPG that reproduces our experimental results. The results may provide novel insights into the organization of spinal locomotor networks.

(Resubmitted 13 July 2012; accepted 5 August 2012; first published online 6 August 2012)

Corresponding author R. M. Harris-Warrick: Department of Neurobiology and Behavior, Cornell University, W 159 Seeley G. Mudd Hall, Ithaca, NY 14853, USA. Email: rmh4@cornell.edu

Abbreviations BES, brain electrical stimulation; CFP, cyan fluorescent protein; CIN, commissural interneuron; CPG, central pattern generator; MLR, midbrain locomotor region; MN, motoneuron; PF, pattern-forming; RG, rhythm-generating.

Introduction

The spinal cord of vertebrates contains special neural networks, called central pattern generators (CPGs), which can organize rhythmic locomotor activity in the absence of supraspinal and sensory inputs (Graham-Brown, 1911; Grillner, 1981, 2006; Kiehn, 2006; Jankowska, 2008; Goulding, 2009). Recently developed genetic methods have been used to identify and characterize multiple interneuron types that are involved in CPG operation (Lanuza *et al.* 2004; Butt *et al.* 2005; Hinckley *et al.* 2005; Wilson *et al.* 2005; Gosgnach *et al.* 2006; Crone *et al.* 2008, 2009; Zhang *et al.* 2008; Kwan *et al.* 2009; Zagoraiou *et al.* 2009; Dougherty & Kiehn, 2010; Zhong *et al.* 2010). However, the overall organization of the locomotor CPG and the pattern of synaptic interconnections between the key interneuron types remain largely unknown.

One way to study the organization of a neural network is to analyse the consequences of perturbations that disturb its output. In the case of the locomotor CPG, which generates a rhythmic locomotor pattern with alternating activity of antagonist motoneuron groups, one class of such perturbations is motor 'deletions'. Deletions are spontaneous errors in the rhythmic locomotor pattern when a set of synergist motoneurons (for example flexor motoneurons on one side) loses rhythmic firing or falls silent during a time period when they are normally active. Deletions were observed during cat locomotion (Duyssens, 1977; Grillner & Zangger, 1979) and were analysed in detail during turtle scratch (Stein & Daniels-McQueen, 2002, 2004; for review see Stein, 2008). Lafreniere-Roula & McCrea (2005) recently studied deletions during fictive locomotion and scratch in the decerebrate cat. They found that deletions in activity of one set of synergist motoneurons (for example, hindlimb extensors) were usually accompanied by either sustained activity or continuing bursting in antagonist ipsilateral motoneurons

(for example hindlimb flexors). Interestingly, during the majority of these deletions, the phase of the rhythm after the deletion did not change, i.e. the rhythmic activity resumed after an integer number of missed cycles. These deletions were called *non-resetting* deletions. A minority of deletions (called *resetting*) did show rhythm resetting which was recognized by a shift in the phase of the motor bursts after the deletion.

Rybak and McCrea proposed a computational model of the mammalian locomotor CPG that could reproduce these results and explain the origin of resetting and non-resetting deletions (Rybak *et al.* 2006*a,b*; McCrea & Rybak, 2007, 2008). In this model, the locomotor CPG has two functional levels: a half-centre rhythm generator (RG), performing a 'clock' function and determining the rhythmic output of the system (oscillation frequency, phase durations), and pattern formation (PF) networks, which receive rhythmic drive from the RG and coordinate the phasing and intensity of activity of the different motoneuron populations. The concept of a two-level CPG organization containing separate RG and PF networks had been suggested by a number of previous studies (Perret & Cabelguen, 1980; Kriellaars *et al.* 1994, reviewed by McCrea & Rybak, 2008; Guertin, 2009) and experimentally supported by other studies (Guertin *et al.* 1995; Perreault *et al.* 1995; Lafreniere-Roula & McCrea, 2005, reviewed by Guertin, 2009). According to the Rybak-McCrea model, failure of activity at the RG level should generally result in a resetting deletion, while failure of activity at the PF level should result in a non-resetting deletion. Therefore, this two-level CPG model could reproduce all the resetting and non-resetting deletions observed during fictive locomotion in decerebrate adult cats (Rybak *et al.* 2006*a*; McCrea & Rybak, 2007).

In this study, we analysed spontaneous deletions occurring during fictive locomotion in the isolated neonatal mouse spinal cord. Unlike the previous work

in the decerebrate cat, we monitored flexor and extensor motoneuron activity on the ventral roots from both left and right sides of the spinal cord. We found that there is a marked asymmetry in the pattern of antagonist motoneuron activity during non-resetting flexor deletions as opposed to extensor deletions in the neonatal mouse spinal cord. We also found that non-resetting spontaneous deletions on one side of the cord were almost never accompanied by disturbances in rhythmic motor activity on the other side of the cord. Simultaneously, we were able to record the activity of several classes of identified spinal interneurons and motoneurons, and investigate their behaviour during non-resetting flexor deletions observed during evoked fictive locomotion. Based on the analysis of these deletions we propose a computational model that can reproduce, and suggest explanations for, our experimental results. Our study may provide insights into the organization of the locomotor CPG in the neonatal mouse spinal cord.

Methods

Spinal cord preparations with and without attached brainstem

Experiments were performed using the isolated spinal cord, with or without brainstem attached, from neonatal (postnatal day (P)P0–P3) wild-type ICR strain or *Chx10::eCFP* mice, which were generated from the ICR strain, and the Chx10 interneurons in the spinal cord are genetically labelled with cyan fluorescence proteins (CFP) (Zhong *et al.* 2010). The animal protocol was approved by the Institutional Animal Care and Use Committee at Cornell University and was in accordance with National Institutes of Health guidelines. The spinal cord dissection without brainstem attached was performed as described previously (Zhong *et al.* 2006a,b, 2007). Briefly, neonatal mice were decapitated and eviscerated in cold oxygenated (95% O₂ and 5% CO₂) low-calcium Ringer solution composed of 111 mM NaCl, 3.08 mM KCl, 25 mM NaHCO₃, 1.18 mM KH₂PO₄, 3.5 mM MgSO₄, 0.25 mM CaCl₂ and 11 mM glucose. The spinal cord, extending from T8/9 to S3/4, was removed and pinned dorsal-side-up in a recording chamber superfused with oxygenated Ringer solution, composed of 111 mM NaCl, 3.08 mM KCl, 25 mM NaHCO₃, 1.18 mM KH₂PO₄, 1.25 mM MgSO₄, 2.52 mM CaCl₂ and 11 mM glucose. To visualize the V2a interneurons in the spinal cord, we removed a small dorsal part of the L2 segment with fine scissors during the dissection. In the brainstem–spinal cord preparation, after evisceration, a piece of the skull was removed and a rostral cut was made between the mesencephalon and the diencephalon; the brainstem and attached spinal cord were carefully isolated, bilaterally intact (Zhong *et al.* 2011). The preparation was pinned

dorsal-side-up in the lumbar spinal cord region, while the brainstem was positioned ventral-side-up by twisting the thoracic/cervical segments by 180 deg. With these manipulations, we were able to record the membrane properties of V2a interneurons from the cut dorsal surface in the lumbar region while electrically stimulating the ventral brainstem area to trigger the fictive locomotion. All experiments were performed at room temperature (20–23°C).

Fictive locomotion in isolated spinal cord

We recorded extracellular motoneuron activity with fire-polished glass suction electrodes on the ventral roots. Fictive locomotion, characterized by the alternation of left/right and ipsilateral flexor (L2)/extensor (L5) ventral root activity, was triggered in two different ways. First, NMDA (5–10 μM) and 5-HT (5–10 μM) were superfused over the recording chamber, reliably inducing fictive locomotion in the isolated spinal cord. Second, fictive locomotor activity was induced by tonic electrical stimulation of the brainstem. An ACSF-filled glass electrode, with a tip diameter of ~100 μm, was placed on the ventral surface of the brainstem, and tonic brain electrical stimulation (BES) was applied (2–4 Hz, 4–5 ms, 1–5 mA). Rhythmic locomotor activity was triggered after 3–8 s of stimulation. In this series of experiments, one recording suction electrode was placed on the ipsilateral L2 (iL2) ventral root to monitor BES-induced fictive locomotion. Rhythmic burst activity from the ventral root was bandpass-filtered (100 Hz to 1 kHz). The fictive locomotion from neonatal *Chx10::eCFP* spinal cord is comparable to that wild-type (Zhong *et al.* 2010).

Electrophysiological recording from spinal interneurons and motoneurons

Commissural interneurons (CINs) and motoneurons (MNs) were recorded from isolated wild-type neonatal mouse spinal cords with blind patch clamp recordings. To identify the CIN type, we used two suction electrodes to stimulate the split rostral and caudal hemicords on the opposite side from the intracellular recording. Collision tests were employed to identify whether the recorded neurons were ascending or descending CINs (Zhong *et al.* 2006a,b, 2007). In the current study, only commissural interneurons which showed highly rhythmic activity during NMDA- and 5-HT-induced fictive locomotion were included for analysis. To identify flexor motoneurons, we used a suction electrode to stimulate the ipsilateral L2 ventral root in the same segment as the neuronal recording, and verified the motoneurons with a collision test of orthodromic action potentials evoked by the recording electrode in the soma and antidromic action potentials

evoked by stimulation of the ipsilateral L2 ventral root, as described previously (Zhong *et al.* 2007). V2a interneurons were recorded from the L2 segment of neonatal spinal cords with partial dorsal horn removal from *Chx10::eCFP* mice during fictive locomotion, as described above. Whole-cell recordings were made with electrodes pulled from thick-walled borosilicate glass (WPI, Sarasota, FL, USA) on a vertical puller (Narishige, Japan) with resistances of 6–10 M Ω ; these were lowered through the cut dorsal surface of the L2 segment to V2a interneurons identified by their CFP fluorescence. The pipette solution contained 138 mM potassium gluconate, 10 mM Hepes, 5 mM ATP-Mg, 0.3 mM GTP-Li and 0.0001 mM CaCl₂ (pH adjusted to 7.4 with KOH). The seal resistance obtained before recordings was always greater than 2 G Ω . Patch clamp recordings were made with a Multiclamp 700B amplifier (Molecular Devices, Sunnyvale, CA, USA) and were driven by Clampex (pCLAMP 9, Molecular Devices). Data were filtered at 20 kHz. Intracellular recordings were accepted for analysis if the action potential overshoot was >0 mV.

Data analysis

Clampfit 9.0 (Molecular Devices), Microsoft Excel and Spike2 (Cambridge Electronic Design, Cambridge, UK) were used for data analysis. A cycle of motor nerve activity started with the onset of an iL2 ventral root burst and ended at the onset of the next iL2 burst; these onsets were determined by a custom-made program in Spike2 to detect when the rectified signal exceeded the average noise level between bursts by a preset amount. Data were analysed in preparations that showed stable rhythmic ventral root activity. Individual spinal neurons were recorded for more than 20 min during NMDA/5-HT-induced locomotor-like activity and for more than 5 min during tonic BES-induced fictive locomotion. The extracellular ventral root recordings were rectified and smoothed with a time constant of 0.2 s, and analysed using custom-written programs in Spike2. The relationship between ventral root activity and neuronal membrane potential was quantified by cross-correlation analysis.

The significance of possible changes in cycle period during deletions was determined with statistical analysis as described by Lafreniere-Roula & McCrea (2005). Cycle periods during deletions were compared with five cycle intervals immediately preceding the deletion. The *t* statistic (Lafreniere-Roula & McCrea, 2005) was used to decide whether the deletion cycle period was changed. The running average (\bar{Y}_2) and variance (s_2) of *X*-cycle intervals with sample size of n_2 ($n_2 = 5$) immediately before the deletion were calculated, where *X* was the hypothesized number of cycles present during the deletion (e.g. *X* = 2 for a single burst deletion). The deletion duration (Y_1)

was compared with the average of *X*-cycle intervals (\bar{Y}_2). The *t* statistic for the deletion was calculated according to the following formula:

$$t = \frac{Y_1 - \bar{Y}_2 - (\mu_1 - \mu_2)}{s_2 \cdot \sqrt{\frac{n_2 + 1}{n_2}}},$$

where $\mu_1 - \mu_2$ is the hypothesized difference ($\mu_1 - \mu_2 = 0$). A significance level of $P < 0.05$ with degrees of freedom $n_2 - 1$ was used to determine whether the cycle period during the deletion was not different from the previous cycles, and hence the deletion was defined as a non-resetting deletion; otherwise, the deletion was called a resetting deletion.

To compare the synaptic drive to an identified neuron with the ventral root output, we integrated the area from the neuron's voltage trace above the baseline (minimal voltage) during each cycle and compared it to the integrated area over the same time period under the corresponding smoothed and rectified ventral root burst. Since the units for the integrated neuronal voltage and ventral root activity were different, we normalized the individual values to the maximal values measured in the eight cycles just before and just after the deletion, respectively. The normalized values for the neuronal and ventral root activity were plotted against one another, and the statistical significance of their relation was assessed using linear regression analysis in Origin 8.

Modelling and simulations

Our model was developed using as a basis the earlier spinal locomotor CPG model of Rybak *et al.* (2006a); the original model simulated locomotor rhythm generation in the immobilized decerebrate cat during fictive locomotion evoked by electrical stimulation of the brainstem midbrain locomotor region (MLR). The two-level structure of the CPG in each hemicord and the architecture of network interactions below the rhythm generator (RG) level, i.e. between ipsilateral populations representing the pattern formation (PF) networks and populations of Ia interneurons, Renshaw cells and motoneuron populations, are the same in the present model as in the preceding model (Rybak *et al.* 2006a). The major changes in the present model include: (i) inclusion of two symmetrical circuits representing the left and right CPGs, interacting via commissural interneurons (CINs) synapsing at the rhythm generator (RG) level; (ii) the RG on each side has an intrinsically rhythmic flexor half-centre and a non-rhythmic extensor half-centre; and (iii) there is no 'supra-spinal drive' imitating MLR stimulation; instead, fictive locomotor activity is initiated by the elevated neuronal excitability that simulates the effect of application of NMDA and 5-HT evoking rhythmic locomotor-like

activity in the isolated spinal cord. The architecture of the model is described in detail in Results, and the equations implementing the model and model parameters are given in Appendix.

All neurons were modelled in the Hodgkin–Huxley style. Interneurons were simulated as single-compartment models. Motoneurons had two compartments: soma and dendrite. As in the preceding Rybak *et al.* (2006a) model, we used the two-compartment motoneuron model proposed by Booth *et al.* (1997). All interneuron types were modelled as in the Rybak *et al.* (2006a) model. However the model parameters were adjusted to (a) make the flexor RG interneuron population on each side to be intrinsically bursting, with frequency of oscillations within the range that seen during fictive locomotion evoked in the isolated neonatal mouse spinal cord by NMDA and 5HT, and (b) elevate excitability of interneurons (defined by the leak reversal potential) so that the locomotor rhythm could be generated without supra-spinal drive imitating the MLR stimulation.

Each neuron type in the model was represented by a population of 50–200 neurons. Heterogeneity of neurons within each population was set by a random distribution of neuronal parameters and initial conditions to produce physiologically realistic variations of baseline membrane potential levels, calcium concentrations, and other parameters of slow channel kinetics. A full description of the model and its parameters can be found in the Appendix. All simulations were performed using simulation package NSM 4.0 developed at Drexel University by S. N. Markin, I. A. Rybak and N. A. Shevtsova. Differential equations were solved using the exponential Euler integration method with a step size of 0.1 ms.

Results

Deletions of motor activity during NMDA/5-HT induced fictive locomotion

Hindlimb locomotor-like activity (fictive locomotion) was induced in the isolated neonatal mouse (P0–P3) spinal cord preparation ($n=66$) by bath application of a mixture of 8 μ M NMDA and 8 μ M serotonin (5-HT). Both wild-type ICR and *Chx10::eCFP* spinal cords were used; the *Chx10::eCFP* strain has no observable behavioural or electrophysiological phenotype (Zhong *et al.* 2010), and fictive locomotion was identical in both strains. Fictive locomotion was characterized by motoneuron burst alternation between the ipsilateral and contralateral segmental ventral roots, and between ipsilateral flexor-dominated (L2) and extensor-dominated (L5) ventral roots on each side of the cord. The bursts of motoneuron activity from the extracellular ventral root recordings were rectified and smoothed, showing peaks of

activity corresponding to each burst (Fig. 1). We observed at least one spontaneous deletion episode during recorded fictive locomotion from 45 of the 66 preparations.

Two examples of flexor deletions seen in recordings from the iL2 are shown in Fig. 1Aa and b. During these deletions, the flexor motoneurons failed to fire, as seen by the absence of the expected peaks of activity (within the areas marked by grey bars) in the smoothed and rectified recordings from the ventral root. During these deletions, the ipsilateral extensor root (iL5) fired continuously

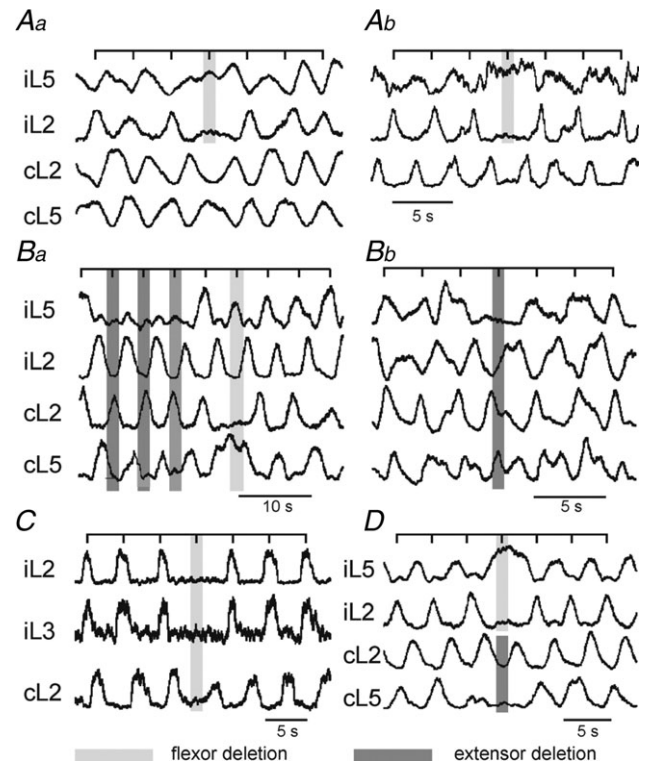


Figure 1. Flexor and extensor deletions during NMDA/5-HT-induced fictive locomotion

All records show smoothed and rectified traces of motoneuron activity recorded extracellularly on the indicated ipsilateral (iL2, iL5) and contralateral (cL2, cL5) lumbar ventral roots. L2 recordings show predominantly flexor motoneuron activity, while L5 recordings show predominantly extensor activity. The bars above each set of traces show the expected timing of the bursts if the rhythm were unperturbed during the deletion. Aa and b, two examples of non-resetting flexor deletions recorded from the L2 root (indicated by the light grey bars) accompanied by tonic activity in the ipsilateral extensor (L5) root, but with no obvious effects on flexor or extensor activity in the opposite side of the cord. Ba and b, multiple non-resetting extensor and flexor deletions from two different spinal cords. Extensor deletions are indicated with dark grey bars, while the single flexor deletion is indicated with a light grey bar. C, a non-resetting flexor deletion occurred simultaneously in ipsilateral L2 and L3 ventral roots, with no effect on contralateral L2 activity. D, the single example of simultaneous deletions on both sides of the cord. A flexor iL2 deletion occurs simultaneously with an extensor cL5 deletion. The iL2 deletion is accompanied by tonic activity in the iL5 ventral root, while cL2 rhythmic bursting is not perturbed during the cL5 deletion. See text for details.

throughout the period when the iL2 failed to burst, and did not show the interruptions in firing normally observed during the ipsilateral flexor bursts.

Figure 1*Ba* and *b* shows examples of extensor deletions, in which extensor bursts (three consecutive deletions in Fig. 1*Ba* and one in panel *Bb*) were missing in the activity of the ipsilateral extensor root (iL5). During these deletions, the corresponding ipsilateral flexor activity (recorded from the iL2 ventral root) retained its normal cyclic bursting.

Most spontaneous deletions in the neonatal mouse spinal cord are non-resetting

Each deletion identified during fictive locomotion was analysed to determine whether it was of a resetting or non-resetting type, using the statistical technique of Lafreniere-Roula & McCrea (2005) as described in Methods. In all, 216 episodes of locomotor activity containing deletions were recorded from 45 spinal cords. Of these, 92% (192) exhibited an integer number of missing cycles ($P > 0.05$) and were characterized as non-resetting. Examples of such deletions are shown in Fig. 1, where the expected cycle timing is shown in the bars above each set of traces. In each case, in the ventral root recording showing a deletion, it resumed bursting at the expected time an integer number of cycles later. The remaining 8% of deletions (24) occurred with rhythm resetting on both sides of the cord; many of these were obtained from cords with irregular locomotor bursting patterns and could reflect the irregularity of the bursting pattern rather than being true resetting deletions. As a result, we focused our analysis on non-resetting deletions in this paper (an example of a resetting deletion is described later in the paper). The percentage of non-resetting deletions in the neonatal mouse spinal cord was larger than that found in the cat (64%; Lafreniere-Roula & McCrea, 2005), suggesting that it is more difficult to perturb the rhythm-generating kernel in the isolated neonatal mouse spinal cord than in the decerebrate adult cat *in vivo*.

Asymmetry in antagonist motoneuron activity during ipsilateral flexor and extensor deletions

Of the 216 deletions found in our recordings, 56% (121) were flexor deletions while 44% (95) were extensor deletions. There was a marked asymmetry in the motor activity of antagonist motoneurons during flexor *vs.* extensor deletions. During all of the flexor deletions (missing bursts in the activity of the iL2 ventral root), the ipsilateral extensor root (iL5) exhibited sustained activity with no interruptions at the times of the missing flexor bursts (see Fig. 1*Aa* and *b*). Similar results were seen in the remaining 119 episodes with flexor deletions. In

contrast, during all extensor deletions (missing bursts in the activity of the iL5 root), the ipsilateral flexor root (iL2) continued unperturbed bursting (see Fig. 1*Ba* and *b*). Figure 1*Ba* shows an example of a non-resetting deletion of three sequential bursts in the iL5 extensor root. Despite this long extensor silence, the iL2 flexor root continued bursting, with unaltered cycle frequency and burst amplitude. Similar results were seen in the remaining 93 episodes with extensor deletions. Note that Fig. 1*Ba* also shows a non-resetting flexor deletion in the activity of the contralateral flexor root (cL2) (highlighted by the light grey bar). As expected, this flexor deletion was accompanied by sustained activity in the contralateral extensor root (cL5). In four preparations, we recorded the activity from both the iL2 flexor root and the adjacent iL3 ventral root, which normally also carries predominantly flexor motoneuron axons. In all four cases, a deletion in the iL2 ventral root was also seen in the iL3 ventral root; an example is shown in Fig. 1*C*. These results suggest that deletions occur simultaneously in motor activity across more than one spinal segment.

Spontaneous non-resetting motor deletions on one side of the cord are independent of contralateral motor activity

The locomotor phase maintenance following non-resetting flexor and extensor deletions, as well as the persistence of ipsilateral flexor bursting during extensor deletions and the sustained extensor activity during flexor deletions, reflects local circuit interactions within the ipsilateral hemicord. However, the activity of these local circuits could also be affected by inputs from the contralateral hemicord. We tested this possibility in several ways.

First, we recorded from the L2 and L5 ventral roots on both sides of the cord, as shown in Fig. 1. These experiments showed that almost all spontaneous non-resetting deletions (except for the single case in Fig. 1*D* and described below) occurring on one side of the cord were not accompanied by disturbances in rhythmic activity on the opposing side. Thus in Fig. 1*Aa* and *b*, deletions of flexor bursts in the iL2 root are accompanied by sustained activity in the ipsilateral iL5 roots, but there are no marked changes in activity recorded from the contralateral cL2 or cL5 roots. Similarly, extensor deletions in Fig. 1*Ba* and *b* are not accompanied by disturbances in ipsilateral rhythmic flexor activity and also do not show disturbances in contralateral flexor and extensor bursting. Of the 192 episodes with non-resetting deletions, only one broke this rule. This single case is shown in Fig. 1*D*, where a flexor deletion in the ipsilateral flexor root (iL2) occurred simultaneously with an extensor deletion in the contralateral extensor (cL5) root. Both

deletions occurred without a significant phase shift after the deletion ($P > 0.05$) and hence were formally classified as non-resetting. It is interesting to note that the rules for relations of ipsilateral flexor–extensor activity during these deletions were followed in each side even in this exceptional case: the iL2 flexor deletion was accompanied by sustained activity in the iL5 extensor root, while cL2 flexor bursting was not perturbed during the cL5 extensor deletion. A possible explanation for this exceptional deletion is given in Discussion. All other spontaneous non-resetting deletions in our experiments were limited to one side of the cord and were not accompanied by disturbances of rhythmic activity on the other side.

To further test the idea that non-resetting motor deletions on one side of the cord are not dependent on input from the contralateral cord, we recorded rhythmic motor activity from isolated left or right hemicords ($n = 11$). Fictive locomotion in an isolated hemicord was induced by NMDA and 5-HT (Bonnot *et al.* 2002; Falgairolle & Cazalets, 2007), though more time was required to stabilize the hemicord rhythmic bursting, and it had a much longer cycle period (around 10 s) than intact spinal cord preparations. We observed 15 episodes of deletions from seven hemicord preparations. Similar to the intact cord, 60% of the deletions (9 of 15) exhibited a failure of flexor activity while 40% were classified as typical extensor deletions; all of these were non-resetting deletions. In these isolated hemicord preparations, the same rules of ipsilateral flexor–extensor interactions during the deletion were observed. Specifically, burst deletions seen in the flexor root were accompanied by sustained activity in the extensor root, while extensor deletions were not accompanied by disturbances of rhythmic flexor activity. Figure 2A shows a non-resetting flexor deletion in the L2 root ($P > 0.25$) accompanied by sustained activity in the L5 extensor root. Figure 2B shows a hemicord recording with three deletions. The first flexor deletion in the L2 root was accompanied by sustained activity in the L5 extensor root; the two subsequent extensor deletions seen in the L5 root were not accompanied by disturbances of L2 bursting.

To identify the minimal region of the cord that can give rise to these deletions, we recorded activity from isolated single L2 hemisegments ($n = 5$). With these hemisegments, a longer time of perfusion with NMDA/5-HT (more than 1 h) was needed to evoke stable rhythmic activity, and the cycle period was very slow (tens of seconds; see Fig. 2C). We observed six episodes of deletions from three single L2 hemisegments which expressed stable rhythmic activity. The deletion shown in Fig. 2C is a non-resetting flexor deletion, as seen by the tick marks and confirmed by our statistical analysis ($P > 0.1$). The other five deletions were also non-resetting. We did not observe deletions of more than one cycle in isolated hemi-

segments. These results show that the CPG ‘clock’ can be functional within an isolated hemisegment, and that the resumption of activity an integer number of cycles later does not require input from other parts of the spinal cord.

Motoneuron activity during deletions

To begin searching for the origins of deletions within the spinal locomotor networks during fictive locomotion, we used whole cell recordings to monitor the activity of flexor-related motoneurons during NMDA and 5-HT induced fictive locomotion. The identity of the L2 flexor-related motoneurons was verified by a collision test of orthodromic action potentials evoked by the recording electrode in the soma and antidromic action potentials evoked by stimulation of the ipsilateral L2 ventral root (data not shown). During fictive locomotion, the activity of the paired left and right L2 ventral roots was monitored. We made intracellular recordings from 23 motoneurons during fictive locomotion, and detected deletions from 12. During ipsilateral ventral root deletions,

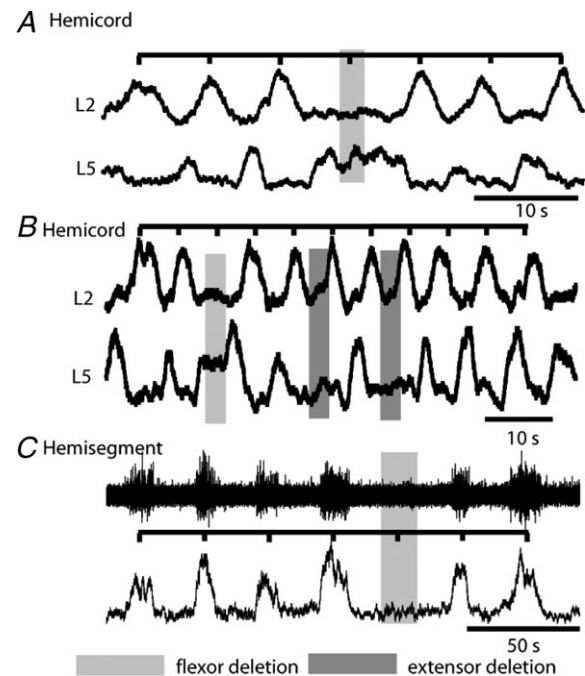


Figure 2. Motor deletions recorded from isolated spinal hemicords and hemisegments

A, a flexor (L2) deletion (light grey bar) during rhythmic activity in the hemicord is accompanied by tonic activity in the L5 extensor root. B, multiple flexor and extensor deletions in a hemicord. The flexor (L2) deletion (light grey bar) is accompanied by tonic extensor (L5) activity, while two extensor deletions (dark grey bars) are not accompanied by perturbation of rhythmic flexor bursting. C, a non-resetting flexor deletion (light grey bar) during NMDA and 5-HT induced rhythmic activity from a single L2 hemisegment.

motoneurons appeared to lose most of their rhythmic synaptic drive and did not fire action potentials. One example during a non-resetting deletion ($P > 0.2$) is shown in Fig. 3A. As seen in this figure, rhythmic changes in synaptic drive to the motoneuron are in phase with the bursts recorded from the ipsilateral ventral root. We analysed the relationship between the motoneuron's synaptically driven rhythmic depolarization during bursts and the corresponding ventral root burst output by integrating the areas under each motoneuron oscillation and the smoothed and rectified ventral root activity, as described in Methods. There was a positive relation between the ventral root area and membrane oscillation area ($n = 16$; $r = 0.32$; $P = 0.031$; Fig. 3B), showing that as the drive to the recorded motoneuron increased, the summed output of the motoneurons recorded on the ventral root also increased. During the deletion, the ventral root area fell close to zero; in parallel, the motoneuron membrane potential became flat and its integrated area also fell close to zero (Fig. 3B). Analysis of intracellular recordings from 11 other flexor motoneurons during 18 episodes containing flexor deletions showed similar positive relationships between the integrated motoneuron area and the integrated ventral root area ($r = 0.36 \pm 0.09$; $n = 12$ neurons), with loss of synaptic drive during an ipsilateral non-resetting flexor deletion. Simultaneous recordings from ipsilateral and contralateral flexor roots demonstrated that rhythmic ipsilateral ventral root activity and the rhythmic synaptic drive to

the ipsilateral motoneuron were not perturbed during contralateral spontaneous flexor deletions. For example, in Fig. 3C, the cL2 ventral root showed three deletions, indicated by the grey bars. No corresponding disturbances were seen in the rhythmic iL2 activity or in the rhythmic pattern of synaptic drive to the iL2-related motoneuron. Similar results were seen in six motoneurons during 10 locomotor episodes with deletions recorded in the contralateral cL2 ventral root. These results suggest that flexor deletions result from a perturbation in ipsilateral premotor circuits, which can greatly reduce or eliminate the synaptic drive to flexor motoneurons. We have not yet performed parallel experiments with extensor-related motoneurons.

Activity of commissural interneurons during locomotor deletions

Commissural interneurons (CINs) send their axons to the opposite side of the cord and coordinate left–right alternation (Butt *et al.* 2002; Butt & Kiehn, 2003; Quinlan & Kiehn, 2007). We recorded CIN activity using blind patch recordings along with iL2 and cL2 ventral root recordings during NMDA/5-HT-induced fictive locomotion. As found previously (Butt *et al.* 2002, 2003; Zhong *et al.* 2006a,b; Quinlan & Kiehn, 2007), a subset of the CINs received strong rhythmic synaptic drive to generate rhythmic bursts of action potentials during fictive locomotion. We performed intracellular recordings from six highly rhythmic CINs during locomotor episodes with at least one deletion in the ipsilateral flexor iL2 activity. Five of these CINs received predominantly rhythmic excitatory synaptic inputs which induced membrane oscillations in phase with the iL2 during fictive locomotion; thus they were flexor-related CINs. One such example is shown in Fig. 4A. This CIN showed rhythmic membrane potential oscillations with occasional action potentials in phase with rhythmic iL2 root activity. The grey area from Fig. 4A is expanded in Fig. 4B, showing a flexor deletion in the iL2 ventral root. The oscillations in this CIN were unperturbed during the deletion in the ipsilateral ventral root. We measured the integrated locomotor burst areas for both ventral root and intracellular CIN recordings. Unlike the motoneurons, we did not find any relation between these areas ($n = 16$; $r = 0.03$; $P = 0.51$; Fig. 4C). In particular, when the ventral root integrated area fell near to zero during the deletion, the normalized CIN area was unaffected. Similar results were seen in four other CINs during a total of 11 ipsilateral deletions ($r = 0.04 \pm 0.02$ for correlation between integrated CIN area and integrated ventral root area; $n = 4$ neurons). The sixth CIN received predominantly rhythmic inhibitory input; we did not perform detailed analysis on this single neuron.

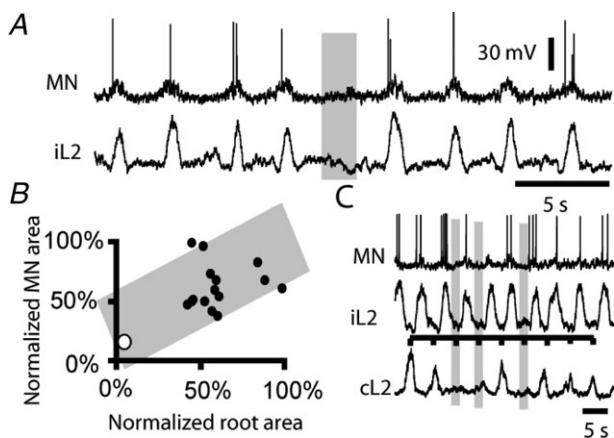


Figure 3. Loss of synaptic drive to flexor motoneurons during non-resetting flexor deletions during NMDA/5-HT-induced rhythmic activity

A, a flexor motoneuron loses its rhythmic depolarization and falls silent during a non-resetting flexor deletion (grey bar). B, there is a significant positive correlation between the integrated ipsilateral ventral root activity during a burst and the integrated membrane potential oscillation of the motoneuron. During the ventral root deletion, the motoneuron displays almost no oscillation. The deletion site is shown as the larger open circle. C, rhythmic synaptic drive and firing of a different flexor motoneuron is unaffected during three contralateral cL2 ventral root deletions.

Two classes of V2a interneurons identified by different behaviour during locomotor deletions

We next studied the activity of the genetically defined V2a interneurons during locomotor deletions. These Chx10-expressing, ipsilaterally projecting, glutamatergic neurons are thought to provide synaptic drive to CINs (Al-Mosawie *et al.* 2007; Lundfald *et al.* 2007; Crone *et al.* 2008) and play important roles in maintaining left–right alternation at high frequencies (Crone *et al.* 2008, 2009; Zhong *et al.* 2010, 2011). Some V2a interneurons may also provide excitatory drive to ipsilateral motoneurons (Lundfald *et al.* 2007; Crone *et al.* 2008; Dougherty & Kiehn, 2010). About half of V2a interneurons are rhythmically active during fictive locomotion (Dougherty & Kiehn, 2010; Zhong *et al.* 2010). In this study, we recorded the activity of 19 rhythmic L2 V2a interneurons which fired in phase with the iL2, each during fictive locomotion episodes containing at least one flexor deletion in the iL2 ventral root activity. Depending on their activity during ipsilateral ventral root deletions, these V2a neurons fell into two distinct groups. A majority of V2a interneurons ($n = 11$), which we called *type I V2a* interneurons, continued to oscillate regularly during 16 episodes of deletions (Fig. 5). In contrast, the remaining eight V2a interneurons, which were called *type II V2a* interneurons, lost their synaptic drive and showed no membrane oscillations during 11 episodes of deletions (Fig. 6).

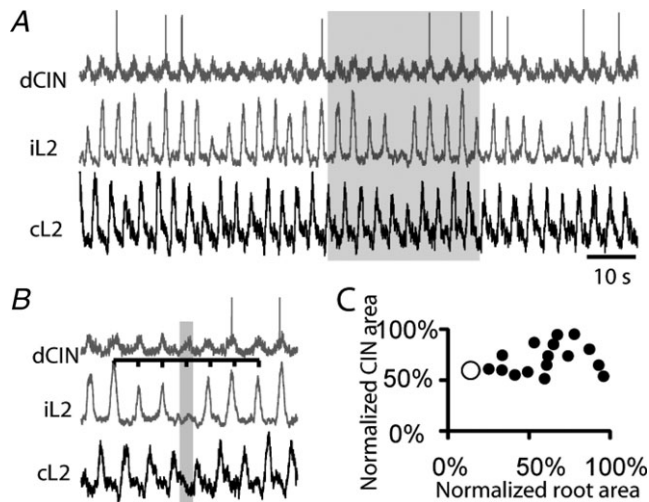


Figure 4. Activity of a flexor-related commissural interneuron (CIN) during a non-resetting flexor deletion

A, the CIN shows rhythmic membrane potential oscillations in phase with the iL2 root activity, and continues to oscillate during flexor deletion. *B*, enlargement of the grey area in *A*, showing the flexor deletion (light grey bar). *C*, there is no significant relation between the integrated iL2 ventral root activity and the integrated membrane potential oscillation of the CIN. The deletion is indicated by the larger open circle.

Figure 5A shows an intracellular recording from a typical type I V2a interneuron during a fictive locomotion episode including a non-resetting ipsilateral flexor deletion ($P > 0.2$). This neuron's activity was in phase with the ipsilateral flexor root, iL2, and it continued to receive rhythmic synaptic drive and to fire rhythmically during the deletion. In this interneuron, there was no significant relation between the integrated area of the extracellular ventral root bursts and the interneuron's integrated membrane potential; the synaptic drive causing the voltage oscillation was not reduced during the iL2 deletion ($n = 16$; $r = 0.02$; $P = 0.62$; Fig. 5B). Five other neurons classified as type I V2a interneurons fired regularly during the deletions and did not show a relationship between the integrated neuron area and the integrated ventral root area during bursting ($r = 0.03 \pm 0.01$; $n = 6$ neurons). Thus, the synaptic input to this V2a interneuron and its activity were unaffected by the network perturbation producing the ipsilateral flexor motoneuron deletion. We also recorded the synaptic currents in this interneuron using voltage clamp recording at -45 mV (Fig. 5C); like most V2a interneurons, this neuron was driven primarily by rhythmic excitatory synaptic input which was in phase with the iL2 activity (Dougherty & Kiehn, 2010; Zhong *et al.* 2010). During two iL2 flexor root deletions, the synaptic drive to this V2a interneuron was not changed, demonstrating that the presynaptic input to this interneuron was not affected during the iL2 deletion. Figure 5D shows the activity of another type I V2a interneuron during a locomotor episode including a non-resetting flexor iL2 deletion; again the rhythmic synaptic drive to this V2a neuron and its activity were unaffected during the deletion. After washout of NMDA and 5-HT to stop fictive locomotion, both this neuron and the iL2 ventral root became quiescent. However, there were occasional spontaneous prolonged bursts (up to 10 s in duration) of motoneuron activity recorded from the iL2 ventral root (Fig. 5E; see also Hanson & Landmesser, 2003). During these spontaneous, non-locomotor ventral root bursts, the type I V2a interneuron did not receive any synaptic drive, and was silent. This result, combined with the type I V2a neuron's unperturbed rhythmic activity during locomotor-related flexor burst deletions, implies that V2a interneurons of this type are not likely to be the major class of pre-motor interneurons projecting to motoneurons, and instead may be components of the locomotor rhythm generator. Five other neurons classified as type I V2a interneurons were also silent during non-locomotor spontaneous ventral root bursts.

In contrast to the type I V2a interneurons, the type II V2a interneurons exhibited a loss of activity in phase with ipsilateral motoneuron deletions. All neurons of this type recorded in our study received rhythmic synaptic drive and fired action potentials in phase with the flexor-related ipsilateral L2 root. During iL2 deletions, these neurons

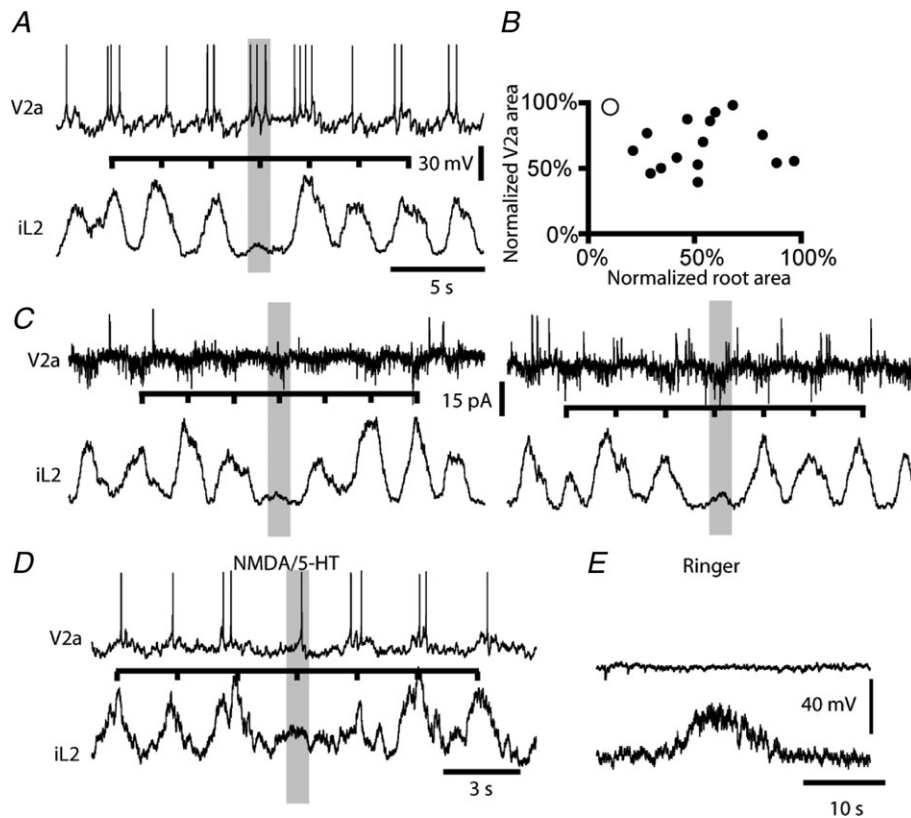


Figure 5. Rhythmic type I V2a interneurons continue to show oscillations and fire rhythmic bursts of action potentials during non-resetting flexor deletions occurring during NMDA/5-HT-induced fictive locomotion

A, a flexor-related V2a interneuron continues to oscillate and fire rhythmically during a flexor iL2 deletion. *B*, there is no significant relation between the integrated iL2 ventral root activity and the integrated membrane oscillations of the V2a interneuron. The deletion is indicated by the larger open circle. *C*, voltage clamp recordings show that this V2a interneuron continues to receive rhythmic excitatory synaptic inputs during two non-resetting iL2 deletions. *D*, another example of continued rhythmic activity of a type I V2a interneuron during an ipsilateral flexor (iL2) deletion. *E*, the type I V2a interneuron from *D* does not receive any synaptic drive during a spontaneous, non-locomotor iL2 burst.

not only were silent but also lost all rhythmic presynaptic drive. For example, the type II V2a interneuron in Fig. 6*A* fired rhythmically in phase with flexor iL2 ventral root activity. During a non-resetting flexor deletion ($P > 0.2$),

this interneuron lost its rhythmic synaptic drive, and fell silent. Unlike the type I V2a interneurons, the integrated voltage oscillation area of this interneuron correlated positively with the integrated area of the extracellular

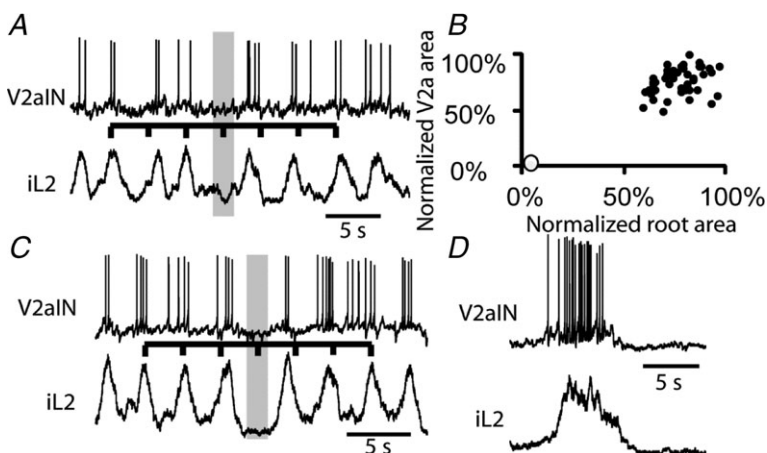


Figure 6. Type II flexor-related V2a interneurons fall silent and lose synaptic drive during flexor deletions during NMDA/5-HT-induced fictive locomotion

A, this V2a interneuron lost its rhythmic synaptic drive during an iL2 flexor deletion. *B*, there is a significant positive correlation between the integrated iL2 ventral root burst amplitude and the integrated membrane potential oscillations of the V2a interneuron from *A*. The deletion is indicated by the larger open circle. *C*, the V2a interneuron in *A* is excited and fires a prolonged burst of action potentials during a spontaneous non-locomotor iL2 burst of activity. *D*, another example of a flexor-related type II V2a interneuron that loses synaptic drive and falls silent during a non-resetting flexor (iL2) deletion.

ventral root bursts ($n = 16$; $r = 0.34$; $P = 0.022$; Fig. 6B). During the iL2 deletion, this interneuron fell silent and its integrated voltage oscillation area fell close to zero, in parallel with the integrated ventral root burst area. A similar loss of synaptic drive was recorded from six other type II V2a interneurons during motor deletions; these neurons all showed a significant positive relation between their integrated area and the integrated ventral root area during locomotor bursts ($r = 0.35 \pm 0.07$; $n = 7$ neurons). Another example of a type II V2a interneuron losing synaptic drive during an iL2 deletion is shown in Fig. 6C. After washout of NMDA and 5-HT, fictive locomotion ceased, and type II V2a interneurons fell silent. However, during rare non-locomotor spontaneous ventral root bursts, these neurons showed strong activation correlated with the motoneuron activation in the iL2 root (Fig. 6D). Thus, the type II V2a interneurons appear to comprise a distinct V2a population which has similar firing patterns to motoneurons during locomotor deletions, and may indeed be pre-motor interneurons (Dougherty & Kiehn, 2010).

Activity of V2a neurons during deletions of brainstem stimulation-evoked fictive locomotion

All the deletions described above occurred during fictive locomotion evoked by bath application of NMDA and 5-HT. Such pharmacologically evoked locomotor-like activity may be considered non-physiological, since it results from non-specific and tonic activation of all NMDA and 5HT receptors in the spinal cord. We needed to make sure that the neuronal behaviours during deletions were not artefacts of the NMDA/5-HT application. To test this, we monitored the activity of interneurons during fictive locomotion evoked by tonic electric stimulation of the brainstem (BES; Zaporozhets *et al.* 2004). BES-evoked fictive locomotion was also characterized by spontaneous deletions similar to those observed during pharmacologically induced fictive locomotion. Over 90% of these deletions were non-resetting, as we found with pharmacologically evoked fictive locomotion. We monitored the activity of five rhythmic V2a interneurons during BES-evoked fictive locomotion: three of these neurons were classified as type I V2a interneurons while two were typical type II V2a interneurons. Figure 7A shows an example of a type I V2a interneuron recorded during a BES-evoked fictive locomotion episode containing a non-resetting flexor deletion in the iL2 root. The activity of this neuron and its synaptic drive were not affected during the flexor deletion. As expected for a type I V2a interneuron, there was no significant relation between the integrated areas of the V2a membrane voltage oscillation and the extracellular ventral root bursts ($n = 16$; $r = 0.09$; $P = 0.27$; Fig. 7B). Similar results were seen for the other

two type I V2a interneurons during BES-induced fictive locomotion. The type II V2a interneurons lost their synaptic drive and fell silent during ipsilateral iL2 deletions (data not shown). We conclude that the behaviour of both types of V2a neurons is independent of the method by which fictive locomotion was produced, and reflects the structural organization of the CPG and the specific roles these interneuron types play in the locomotor CPG network.

Activity of unidentified spinal interneurons during locomotor deletions

During our blind patch experiments, we occasionally recorded the activity of unidentified rhythmically active spinal interneurons during fictive locomotion. We recorded the activity of 12 unidentified neurons which were not CINs, which were rhythmically active in phase with the iL2 flexor motoneurons. During ipsilateral iL2 deletions, 7 of these 12 neurons continued to display rhythmic activity. Figure 8A shows an example of one such neuron during a non-resetting deletion. This neuron continued to oscillate and fire action potentials when the iL2 fell silent. As with the CINs and type I V2a interneurons, this neuron's integrated membrane voltage area showed no significant relation to the integrated ventral root burst areas ($n = 16$; $r = 0.042$; $P = 0.45$; Fig. 8B). Voltage clamp recordings at -45 mV showed that this neuron was synaptically driven by inward synaptic currents in phase with ipsilateral ventral bursts,

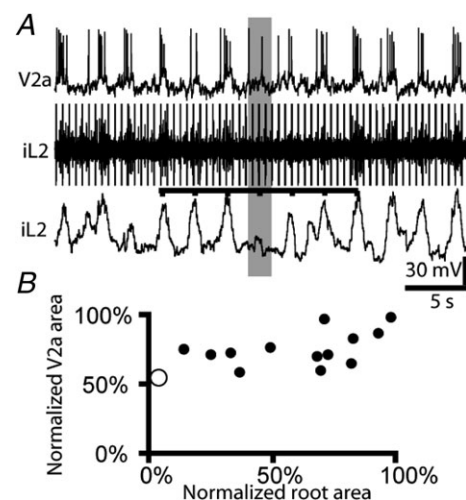


Figure 7. Type I V2a interneurons continue to fire rhythmically during non-resetting deletions occurring during BES-induced fictive locomotion

A, a flexor-related type I V2a interneuron continues to receive rhythmic synaptic drive and fire action potentials during an iL2 deletion. B, there is no significant relation between the iL2 integrated ventral root amplitude and the integrated membrane potential oscillations of the V2a interneuron.

and outward currents during contralateral ventral root bursts (Fig. 8C). Two non-resetting ipsilateral flexor iL2 deletions occurred in this recording, one of which lasted for five consecutive cycles. Both the rhythmic excitatory and inhibitory phases of synaptic drive to this neuron were unaffected during these deletions, and the cycle frequency remained constant (Fig. 8C). The remaining five unidentified interneurons lost their synaptic drive and fell silent during iL2 motor deletions; their firing pattern was similar to the ipsilateral motoneurons and the type II V2a interneurons (data not shown).

A two-level asymmetrical model of the locomotor CPG

We have generated a model of the mouse neonatal locomotor CPG to help interpret our experimental results. Figure 9A shows a schematic diagram of our model of a hemicord locomotor CPG. This model was developed using a combination of two basic concepts: the concept of two-level CPG organization, as previously implemented in the Rybak–McCrea model (Rybak *et al.* 2006a,b; McCrea & Rybak, 2007, 2008), and the Duysens–Pearson concept of an asymmetric rhythm generator with a dominant flexor half-centre or with a pure flexor-related rhythm generator (Pearson & Duysens, 1976). Similar to the Rybak–McCrea model, the present model has two functional/hierarchical levels referred to as the ‘rhythm generator’ (RG) and ‘pattern formation’ (PF) networks. To implement the Duysens–Pearson concept of a flexor-dominant locomotor generator, which is implicitly suggested by our experimental data showing asymmetrical effects of flexor and extensor deletions (Fig. 1), the RG in the current model has only one intrinsically rhythmic half-centre generating a flexor-related rhythmic activity

(RG-F population). As in the previous Rybak *et al.* (2006a) model, bursting in this population is based on a persistent (slowly inactivating) sodium current in each neuron and mutual excitatory synaptic interactions within the RG-F population (the existence of this current in the spinal cord was confirmed by several studies, see Zhong *et al.* 2007; Tazerart *et al.* 2008; Brocard *et al.* 2010; Ziskind-Conhaim *et al.* 2010). The non-rhythmic extensor half-centre (RG-E population) is tonically active. However, its activity contributes to control of the duration of the extensor phase and the timing of switching to the next flexion via the inhibitory In-RG-E population, whose activity is in turn regulated by the rhythmic RG-F half-centre via the inhibitory In-RG-F population. In accordance with the two-level concept, the RG network in this model performs a ‘clock’ function: it defines the locomotor frequency, coordinates left and right rhythmic patterns (via different types of CINs), and drives the activity of the PF network.

The PF network has two principal populations, PF-F and PF-E, which drive locomotor activity in flexor and extensor motoneuron populations, respectively. These populations reciprocally inhibit each other via the In-PF-F and In-PF-E populations and drive alternating activity in the various flexion- and extension-related populations of the ipsilateral locomotor network. The PF-F population receives rhythmic drive from the RG-F rhythm generator and provides rhythmic drive to the flexor motoneurons. The PF-E population receives tonic drive from the RG-E population, and is rhythmically inhibited during the flexor phase by the PF-F neurons via the inhibitory In-PF-F neurons. The PF-E population provides rhythmic drive to the extensor motoneurons, and can help regulate PF-F activity via the inhibitory In-PF-E interneurons.

We have expanded this model to reflect interactions between CPG networks on the left and right sides of the

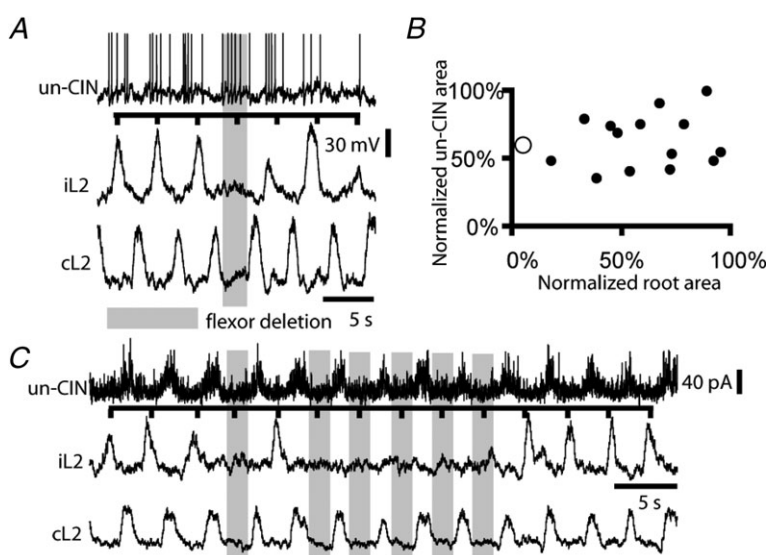


Figure 8. Responses of unidentified neurons during deletions occurring during NMDA/5-HT-induced fictive locomotion

A, an unidentified non-commissural interneuron continues to fire rhythmically during an iL2 deletion. *B*, there is no significant relation between the integrated iL2 ventral root burst amplitude and this neuron's number of action potentials per cycle. The deletion site is indicated by the larger open circle. *C*, voltage clamp recording of synaptic inputs to the neuron from *A* during multiple iL2 deletions. The rhythmic synaptic drive to the neuron is maintained during the deletions.

spinal cord. The schematic diagram of the full model that incorporates interactions between symmetrical circuits in the left and right hemicords is shown in Fig. 9B. The left and right CPGs (each organized as shown in Fig. 9A) interact at the RG level via CIN populations (Butt & Kiehn, 2003). Specifically (see Fig. 9B) the l-CINi-F and r-CINi-F populations provide mutually inhibitory interactions between left and right flexor RG half-centres (l-RG-F and r-RG-F); the l-CINe-F and r-CINe-F populations provide excitatory inputs from each RG flexor half-centre (l-RG-F and r-RG-F) to both contralateral RG half-centres (r-RG-F and r-RG-E, and l-RG-F and l-RG-E, respectively); and the l-CINe-E and r-CINe-E populations provide excitatory input from each extensor half-centre (l-RG-E and r-RG-E) to contralateral flexor half-centres (r-RG-F and l-RG-F, respectively). In addition, inhibitory interactions between ipsilateral flexor and extensor antagonists operate via the inhibitory Ia-F and Ia-E populations, which also inhibit each other and receive inhibition from the corresponding populations of Renshaw cells (R-F and R-E), whose activity shapes firing activity of the corresponding motoneuron pools. Organization of these lower-level interactions is based on a large body of data obtained in previous studies in the cat (McCrea *et al.* 1980; Lundberg, 1981; Shefchyk & Jordan, 1985; Pratt & Jordan, 1987; Jankowska, 1992; Geertsen *et al.* 2011) and was used in the earlier Rybak *et al.* (2006a) model.

Simulation results

The performance of our model under normal conditions and during simulated perturbations producing non-resetting deletions is shown in Fig. 10. In accordance with the two basic concepts described above, a fictive locomotor-like pattern with alternating ipsilateral flexor–extensor and left–right bursting activity is generated in the model by two (left and right) rhythmic flexor half-centres (l-RG-F and r-RG-F) and is coordinated by the interactions between left and right half-centres via the inhibitory and excitatory CIN populations. The architecture of neuronal interactions implemented in the model (Fig. 9B) allows it to generate coordinated flexion-related oscillations at the RG level, and transform these oscillations (through the specific interactions between different neuron populations on each side of the cord) into the left–right and flexor–extensor alternating locomotor-like activity of the corresponding motoneuron populations. The integrated activity of all major populations is shown in Fig. 10.

As an initial test of the functional roles of the CIN-mediated interactions between left and right circuits in the model, we simulated the effect of hemisection, i.e. a full removal of all contralateral circuits and CIN populations. The result of this simulation is shown

in Fig. 11. This figure shows that removal of contralateral circuits in the model reduced the frequency of locomotor oscillation, approximately by half, while maintaining the symmetric ipsilateral flexor–extensor alternation (approximately equal durations of flexor and extensor phases). These simulations closely reproduce our experimental data on the results of hemisection (see Fig. 2A and B and compare with records in Fig. 1). Our analysis has shown that the reduction in locomotor frequency after simulated hemisection results mainly from the elimination of excitatory input to the rhythm-generating ipsilateral RG-F population from the contralateral RG-E population, which may be considered as a prediction for further experimental studies.

We then focused our study on the changes in interneuron and motoneuron rhythmic activity during various deletions, as described by our experimental studies. As indicated in Fig. 9A, deletions could be produced in the model by simulated disturbances evoked by either application of short-duration excitatory or inhibitory signals to particular PF or RG populations or temporary suppression of inputs to these populations. In our simulations, non-resetting flexor and extensor deletions on each side could be produced by simulated perturbations affecting the model at the level of the ipsilateral PF circuits. Examples of simulated perturbations that produce non-resetting deletions are shown in Fig. 10. The first deletion in this figure was produced by a brief suppression of excitatory input from the left RG-E (l-RG-E) to the left PF-E population (l-PF-E), as shown in Fig. 9A by the open arrow. Application of this perturbation is indicated by the bar at the top of the figure and by the dark grey rectangle. This perturbation produced a non-resetting deletion in the activity of the left extensor motoneurons (l-Mn-E, second trace) without disturbing rhythmic activity of the ipsilateral flexor motoneurons (l-Mn-F, top trace) or the CINs and contralateral flexor or extensor motoneurons (two bottom traces). This corresponds to the non-resetting extensor motor deletions observed in our experimental studies (Fig. 1Ba and b). The second disturbance in Fig. 10 (illustrated by the light grey rectangle and the bar at the bottom of the figure) demonstrates a non-resetting flexor deletion occurring on the right side of the cord (two flexor bursts are missed in activity of the right flexor motoneuron, r-Mn-F). This non-resetting deletion was produced by a brief suppression of excitatory input from the right RG-F (r-RG-F) to the right PF-F population (r-PF-F), as shown in Fig. 9A by another unfilled arrow. Similar non-resetting flexor deletion could be also produced by a brief increase of activity (e.g. by an external excitatory drive) to r-PF-E, which would then inhibit the r-PF-F population. This non-resetting flexor deletion was accompanied by sustained activity of ipsilateral (right)

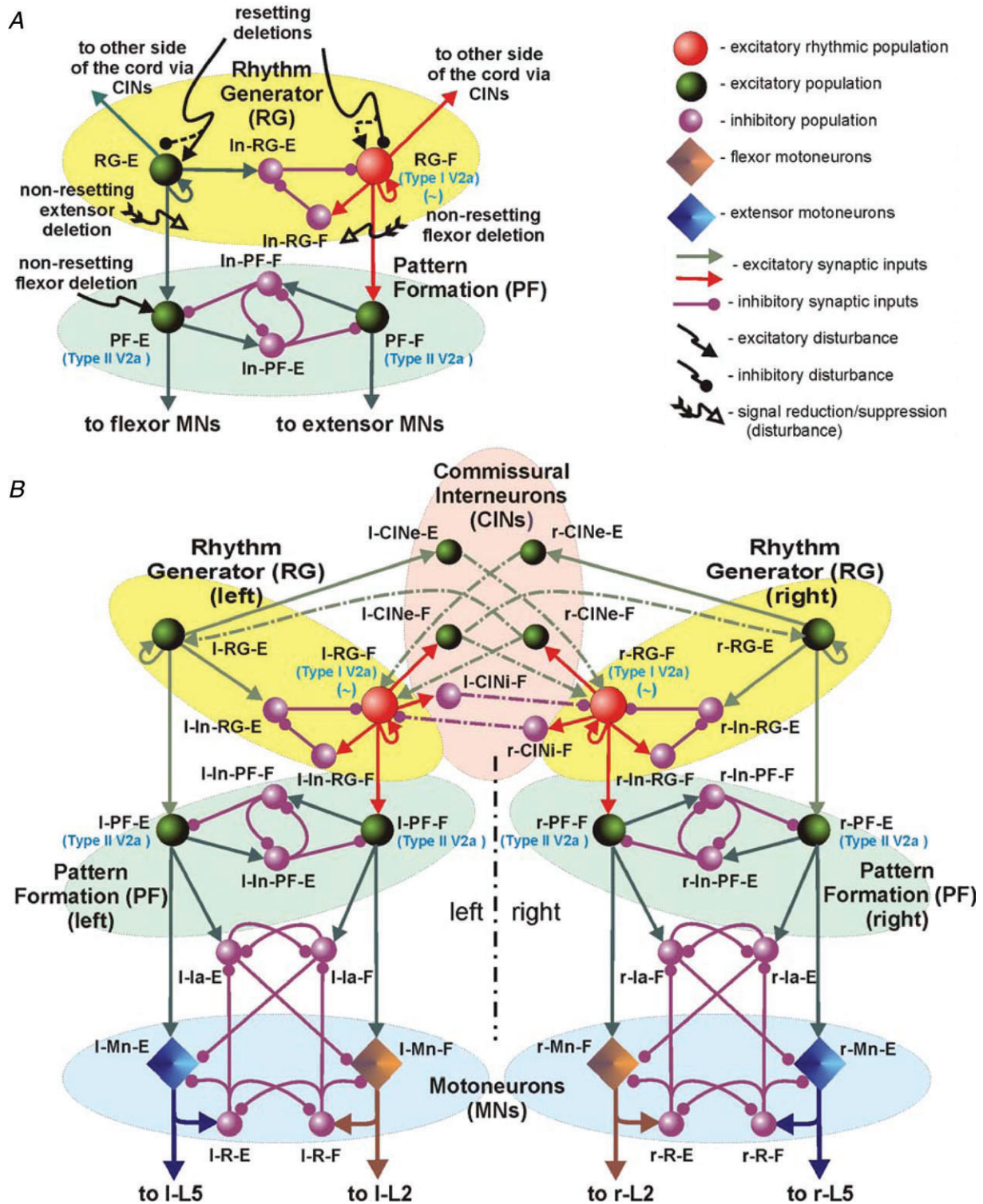
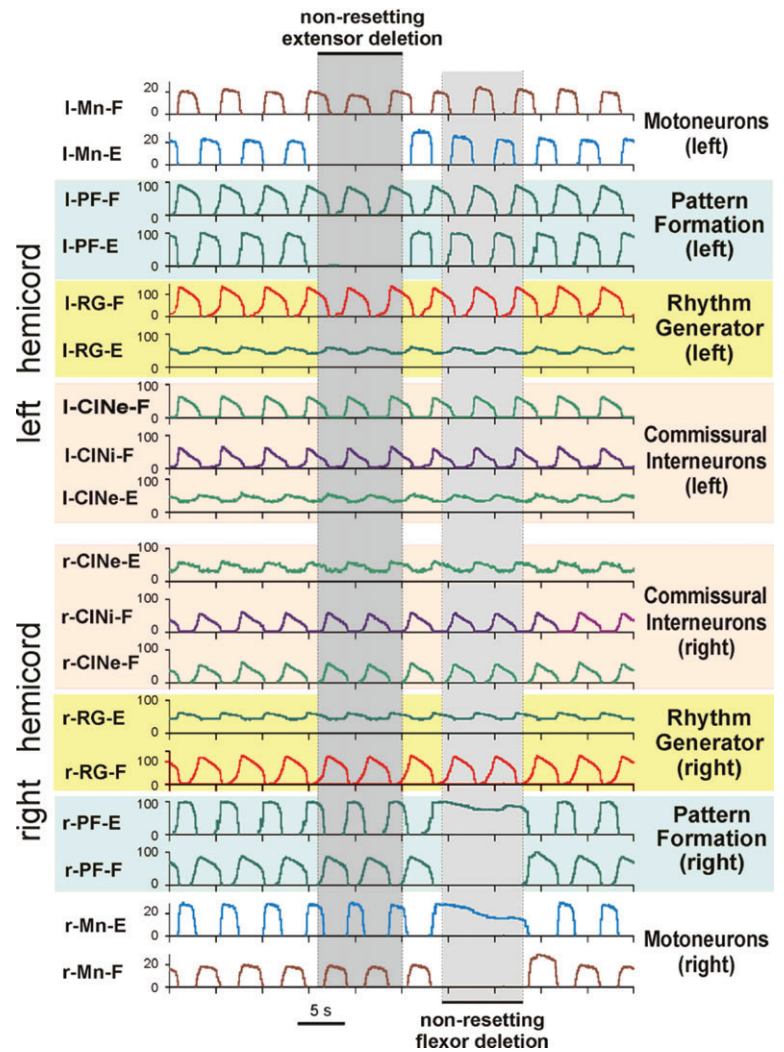


Figure 9. Schematic diagram of the model
 Populations of interneurons are represented by spheres. Excitatory and inhibitory synaptic connections are shown by arrows and small circles, respectively. Populations of motoneurons are represented by diamonds. A, the two-level asymmetrical model of the locomotor CPG generating and controlling rhythmic activity in one hemicord. The CPG consists of a rhythm generator (RG) and a pattern formation (PF) network. The asymmetrical RG has two half-centres: an intrinsically rhythmic flexor half-centre (RG-F population, red sphere), generating flexor-related rhythmic activity, and a tonically active flexor half-centre (green sphere), interacting via inhibitory interneuron populations (In-RG-E and In-RG-F). The PF network contains interneuron populations (PF-F and PF-E, green spheres).

Figure 10. Performance of the model and simulation of non-resetting deletions

Activities of all excitatory populations and CINs in the left and right hemicords are shown. Activity of each population (in this and following figures) is represented by the average histogram of neuronal activity in the corresponding population (number of spikes per second per neuron, bin = 50 ms). The colour of each trace corresponds to the population type (see Fig. 9). The model generates coordinated flexion-related oscillations in each RG and transforms these oscillations into the left–right and flexor–extensor alternating locomotor-like activity of the corresponding motoneuron populations. This simulation shows two non-resetting deletion episodes indicated by the grey rectangles. The first deletion episode represents a non-resetting deletion of left extensor activity accompanied by rhythmic flexor activity (dark grey rectangle). This deletion was produced by a brief removal of excitatory input to the l-PF-E population from the l-RG-E (as shown in Fig. 9A by an open arrow). The applied perturbation is indicated by the bar at the top of the traces. The second deletion episode represents a non-resetting deletion of right flexor activity accompanied by tonically active extensors (see light grey rectangle). This deletion was produced by a brief removal of excitatory input to the r-PF-F population from the r-RG-F (shown in Fig. 9A by the other open arrow). Application of this perturbation is indicated by the bar at the bottom of the traces. During both deletion episodes the activity of the contralateral populations is unaffected. See text for details.



extensor motoneurons (second trace from the bottom) without any disturbances in the rhythmic activity of CINs and contralateral flexor or extensor motoneurons (two top traces). This corresponds to the non-resetting flexor motor deletions observed in our experimental studies (Figs 1Aa and b and 4).

As described above, non-resetting deletions could be produced in the model by perturbations applied to the PF network on one side of the cord, i.e. below the ipsilateral RG circuits and CIN populations. As a consequence, it is not surprising that these perturbations did not disturb rhythmic activity of the CINs and contralateral inter-

neurons and motoneurons. This is consistent with our experimental data showing no effect of non-resetting deletions on CINs and contralateral motoneurons (Figs 3C and 4, respectively).

Although we did not observe many unambiguous examples of resetting deletions in our experiments, such resetting deletions can occur, and have been analysed in the cat (Lafreniere-Roula & McCrea, 2005). Our model can produce resetting deletions, shifting the phase of the following motor bursts, by a perturbation that affects the circuitry at the RG level. Figure 12 shows examples of such simulations using our model. In Fig. 12A, the

that receive inputs from the corresponding RG populations and inhibits each other via the inhibitory populations (In-PF-E and In-PF-F). Possible sources of perturbations producing various resetting and non-resetting deletions are indicated by different arrows (see key). B, schematic diagram of the full locomotor model with bilaterally organised locomotor CPGs interacting via populations of commissural interneurons (CINs). The model has symmetrically organized left and right networks with the identical CPG circuits on each side organized as shown in A. The network in each side also includes Ia interneuron populations (Ia-F and Ia-E), Renshaw cells (R-F and R-E), and flexor and extensor motoneuron populations (Mn-F and Mn-E). Prefix l- or r- in the population names indicates that the population belongs to the left or right hemicord, respectively. See text for details.

applied perturbation, shown at the top (bar), temporarily inhibited the rhythmic l-RG-F population, producing an ipsilateral deletion in flexor motoneurons (l-Mn-F). As in case of non-resetting deletions, this motoneuron flexor deletion was accompanied by sustained activity of ipsilateral extensor motoneurons (l-Mn-E). However, in this example the deletion was resetting (see the phase shift indicated at the bottom of the motoneuron traces). Although the perturbation was applied only to the ipsilateral l-RG-F population, it also affected contralateral activity via the CIN populations projecting to the contralateral RG populations. As a result, the applied perturbation also disturbed the activity of contralateral motoneurons (two bottom traces). Specifically, during

the deletion of the ipsilateral l-RG-F flexor burst, this population did not inhibit the contralateral flexor burst in r-RG-F via the l-CINi-F population (see Fig. 9B). In addition, the sustained activity of l-RG-E during this deletion additionally excites the contralateral r-RG-F (see Fig. 9B), producing an advanced onset of contralateral flexor bursts in r-RG-F and in the r-Mn-F population, and a partial deletion (reduction in both amplitude and duration) of the right extensor r-Mn-E motoneuron burst. This disturbance also produced some transitional post-perturbation temporal dynamics before returning to the stable oscillations, with an obvious phase shift relative to the initial rhythm.

The simulation in Fig. 12B was specially performed to fit a rare experimentally recorded episode with a clearly resetting deletion, shown in Fig. 12C. In this experiment, regular bursting activity was recorded before and after the resetting deletion. The deletion episode in this experiment is characterized by (a) a partial extensor deletion on the ipsilateral side (in the iL5 root: dark grey bar) and (b) a flexor deletion on the contralateral side (in cL2: light grey bar) that was accompanied by sustained activity in the associated extensor root (cL5). Figure 12B reproduces such a resetting deletion in our model by a brief inhibition applied to the l-RG-E population, shown at the top (bar). This simulated perturbation produced both an ipsilateral extensor deletion (see l-Mn-E) and a contralateral flexor deletion (see r-Mn-F) accompanied by sustained activity in the contralateral extensors (see r-Mn-E). Specifically, suppression of ipsilateral extensor activity in l-RG-E removed inhibition from this population to the ipsilateral flexor half-centre (l-RG-F, via the inhibitory l-In-RG-E population, see Fig. 9B), thus producing an advanced onset of the next ipsilateral flexor burst in l-RG-F. This burst, via the commissural l-CINi-F, strongly inhibited the contralateral (right) flexor RG half-centre (r-RG-F, see Fig. 9B), finally causing the flexor deletion of the contralateral flexor motoneurons (r-Mn-F) accompanied by a sustained activity in right extensor motoneurons (r-Mn-E). As indicated in Fig. 12B, and similar to the corresponding experimental episode in Fig. 12C, these deletions shift the phase of subsequent bursts and thus are of the resetting type.

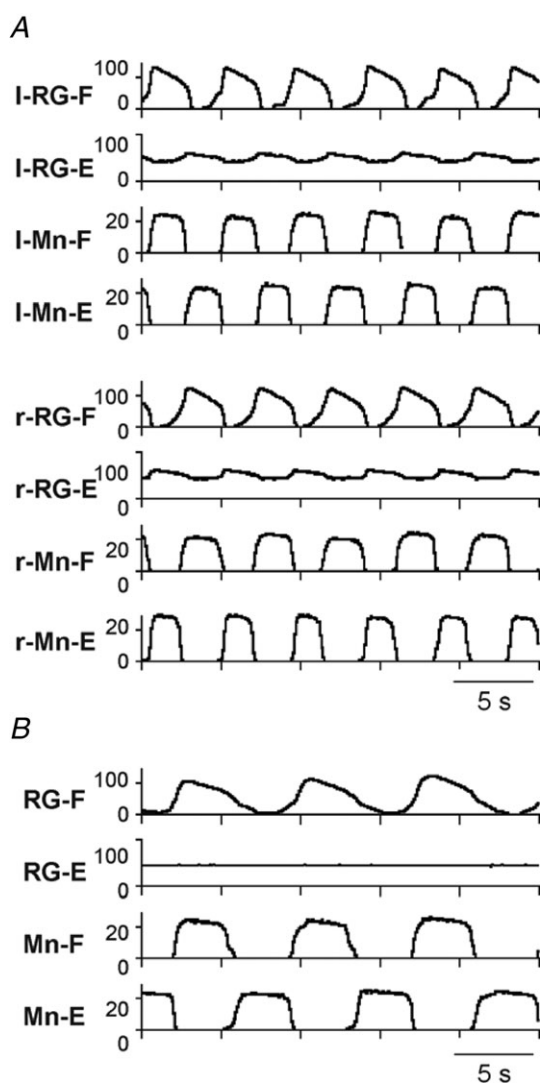


Figure 11. Simulation of hemisection

A, activity of the principal RG populations and motoneuron populations in the intact model. B, changes in the activity of the same populations after simulated hemisection (removal of all circuits located in the right hemisection). See text for details.

Discussion

Spontaneous deletions in rhythmic locomotor activity in the neonatal mouse spinal cord

Analysis of spontaneous motor deletions during MLR-evoked fictive locomotion in the decerebrate, immobilized cat showed that about two-thirds of deletions were non-resetting, suggesting that they did not result from perturbations in the rhythm-generating (RG) kernel of the CPG (Lafreniere-Roula & McCrea, 2005; Rybak *et al.*

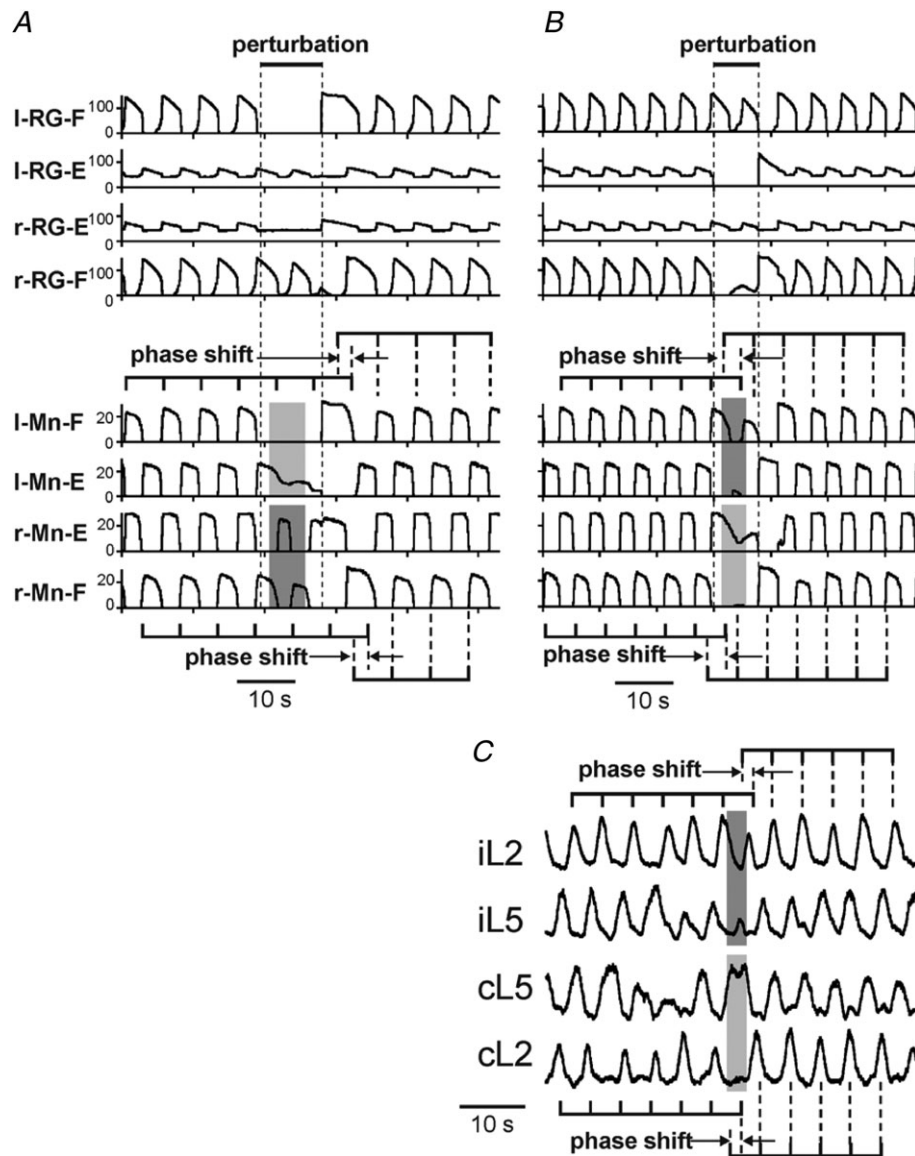


Figure 12. Simulation of resetting deletions

A, rhythm disturbance was produced by a brief inhibition of the I-RG-F population (indicated by a bar above the traces). This perturbation produced a resetting flexor deletion in the left flexor motoneuron activity (I-Mn-F population) accompanied by a sustained activity in left extensor motoneurons (I-Mn-E population) (marked by a light grey rectangle). Although applied to the left RG, this perturbation also affected the activity of the contralateral (right) RG (via commissural interneurons, not shown) and finally perturbed the activity of right extensor and flexor motoneurons (r-Mn-F and r-Mn-E populations) (marked by a dark grey rectangle). As indicated in the figure, the applied perturbation produced a phase shift after resumption of rhythmic motoneuron activity in both sides. B, in this example the rhythm was disturbed by a brief inhibition of the I-RG-F population (shown as a bar at the top). This perturbation produced an ipsilateral partial deletion in the extensor motoneurons (see I-Mn-E trace) (indicated by dark grey rectangle) and a contralateral flexor deletion on the right side (see r-Mn-F trace) accompanied by sustained extensor activity (r-Mn-E trace) (marked by the light grey rectangle). Rhythmic activity resumed with an identical phase shift on both sides. This simulation was specifically performed to reproduce the experimental episode of a resetting deletion shown in panel C below. C, an experimentally recorded episode with a resetting deletion. An unknown perturbation produced a partial extensor deletion on the ipsilateral side (in the iL5 root) and a flexor deletion on the contralateral side (in cL2) that was accompanied by sustained activity in the extensor cL5. In all panels (A–C), the horizontal bars with vertical ticks located above and below motoneuron traces indicate the timing of locomotor periods before and after deletions, allowing the visualization of the phase shift between the initial and resumed rhythms. See text for details.

2006a). Our experiments in the isolated neonatal mouse spinal cord show that the percentage of non-resetting deletions (92%) is even larger than in the decerebrate cat. This suggests that the RG network in this preparation is more resistant to resetting than in the adult cat *in vivo*. This difference does not appear to result from different methods used to evoke fictive locomotion. While most of our experiments with the neonatal mouse spinal cord evoked fictive locomotion by application of NMDA and 5-HT, we found the same high frequency of non-resetting deletions during BES-evoked fictive locomotion. The different ages and species of the animals (adult cat *vs.* neonatal mouse) might explain the greater resistance to locomotor rhythm resetting in the neonatal mouse.

Our results show that in the isolated neonatal mouse spinal cord, spontaneous locomotor deletions on one side of the cord are normally not accompanied by rhythm disturbances on the opposite side. Non-resetting deletions can occur in an isolated hemicord, showing that maintenance of the rhythm phase during the deletion does not require inputs from the opposite side of the cord. Our results confirm that each hemicord contains an independent rhythmogenic network that can function in the absence of the other hemicord, although the left and right networks are normally coupled via commissural interneurons. We have also shown that locomotor oscillations with non-resetting deletions occur even in an isolated hemisegment. This confirms the distributed nature of the rhythmogenic components of the CPG, as previously shown by lesion studies (Cazalets *et al.* 1995; Kjaerulff & Kiehn, 1996; Cowley & Schmidt, 1997; Kiehn & Kjaerulff, 1998).

Firing properties of spinal neurons during motor deletions

The neonatal mouse spinal cord preparation offers a unique opportunity to monitor the activity of identified classes of neurons during locomotor deletions. We recorded the activity of motoneurons and two types of identified interneurons thought to be involved in locomotor pattern generation, V2a interneurons and CINs, during locomotor deletions. As expected, the firing activity and integrated membrane potential oscillations of motoneurons projecting to the ipsilateral ventral roots correlated with the root's integrated activity; deletions of ventral root activity always accompanied a loss of synaptic drive and failure to fire in the corresponding motoneurons (Fig. 3). This suggests that the last-order interneurons providing the synaptic drive to motoneurons also fall silent during deletions.

Our experiments reveal the existence of two functional subtypes of V2a interneurons with different behaviours during ipsilateral flexor deletions. Rhythmic activity in the

type I V2a interneurons was not perturbed during flexor deletions in the ipsilateral ventral root. The integrated synaptic drive to these neurons did not correlate with the integrated motor output, and did not decrease during the ventral root deletion. In addition, the type I V2a interneurons remained silent during spontaneous ipsilateral ventral root bursts in the absence of fictive locomotion. We suggest that the type I V2a interneurons do not provide direct synaptic drive to motoneurons, but are instead involved (directly or indirectly) in rhythm generation and/or coordination between left and right networks via the CINs. This class could, for example, constitute the V2a interneurons that form anatomically defined synapses on the V0 CINs (Crone *et al.* 2008).

In contrast to type I V2a interneurons and similar to motoneurons, the type II V2a interneurons fell silent during non-resetting ipsilateral flexor deletions. Moreover, they lost locomotor related synaptic drive during these deletions, and their integrated membrane potential oscillations correlated positively with the integrated bursts of the corresponding ipsilateral ventral root. In addition, they fired at high frequency during spontaneous ipsilateral ventral root bursts in the absence of fictive locomotion. These results suggest that the type II V2a interneurons do not belong to the RG circuits (whose activity is not perturbed during non-resetting deletions), but can be components of the pattern formation network and/or last-order interneurons that directly project to motoneurons (Lundfald *et al.* 2007; Crone *et al.* 2008; Dougherty & Kiehn, 2010). The loss of synaptic drive to these neurons during non-resetting deletions suggests that the higher order interneurons which drive them also fall silent during these deletions.

The commissural interneurons (CINs), which send their axons contralaterally and coordinate phase relationships between left and right locomotor networks, have been shown to display a wide variety of firing properties during fictive locomotion (Butt *et al.* 2005; Butt & Kiehn, 2003; Jankowska *et al.* 2003, 2005; Zhong *et al.* 2006a,b; Quinlan & Kiehn, 2007). We found that all flexor-related rhythmic CINs recorded in our study continued to receive rhythmic synaptic input and to fire rhythmically during non-resetting ipsilateral flexor deletions. This supports the idea that these CINs receive synaptic drive from the ipsilateral rhythm generator, which continues its rhythmic activity during non-resetting deletions. Some of these CINs may also receive excitation from the type I V2a interneurons (Crone *et al.* 2008).

A two-level asymmetrical model of the neonatal mouse locomotor CPG

The phenomenon of non-resetting deletions during fictive locomotion in the cat has previously been explained by a model of a two-level locomotor CPG controlling

each limb, which contains a top-level RG, maintaining the period and phase of locomotor oscillations, and a lower-level PF network operating under control of the RG and driving the activity of motoneuron populations (Rybak *et al.* 2006a, McCrea & Rybak, 2007). According to this model, reciprocal inhibition between antagonistic circuit elements in each hemicord operates at both RG and PF levels. Perturbations at the RG level cause resetting motor deletions, while perturbations at the PF level cause non-resetting motor deletions (Rybak *et al.* 2006a, McCrea & Rybak, 2007). This earlier model, however, did not consider contralateral left–right interactions. To support bilateral interactions, three types of commissural neurons (CIN populations) have been incorporated in our model (see Fig. 9B). Such excitatory and inhibitory CINs have been described experimentally (Cowley & Schmidt, 1995; Butt & Kiehn, 2003; Hinckley *et al.* 2005; Quinlan & Kiehn, 2007), and a subset of the CINs receive strong rhythmic synaptic drive to generate rhythmic activity during fictive locomotion (Butt *et al.* 2002, 2003; Zhong *et al.* 2006a,b; Quinlan & Kiehn, 2007). In our current bilateral two-level model, the commissural interneurons mediate left–right interactions only at the RG level, i.e. between left and right RG interneuron half-centre populations. If this organization is correct, then interneurons that are involved in generation of the locomotor rhythm should demonstrate rhythmic activity during fictive locomotion that should not be perturbed during non-resetting deletions. This could include neurons that belong to the left or right RG, CINs that coordinate interactions between the left and right RGs, and the type I V2a interneurons that could transfer RG drive to the CINs. In addition, however, there may be other types of CINs which are presumably involved in the operation at the PF circuits, which may directly project to motoneurons, as has been previously described (Butt & Kiehn, 2003; Quinlan & Kiehn, 2007). The activity of such CINs is expected to be perturbed during non-resetting deletions. However, such CINs have not been detected in our current study.

One of the major results of this work is that we have indeed found both types of identified interneurons: those that are presumably involved in the operation of RG on each side or in interactions between left and right RGs, and those which instead operate at the PF level. Specifically, the CINs and type I V2a interneurons recorded in our study have the features of interneurons involved in RG operation described above, while the type II V2a interneurons appear to fit to the description of the PF level interneurons. They may belong to PF circuits or represent last-order interneurons organizing the phasing and activity of the corresponding motoneuron populations. In addition, during blind patch recordings, we monitored the activity of 12 other unidentified spinal interneurons which were rhythmically active during fictive locomotion; 7 of these neurons showed no perturbation

during non-resetting motor deletions (suggesting a relation to RG network activity), whereas the remaining five interneurons lost activity during the non-resetting motor deletions (suggesting a relation to PF network activity). All of these results provide support for the concept of a two-level CPG organization.

Another striking result of our current study of the neonatal mouse isolated spinal cord preparation was the finding of strong asymmetry in motor activity during spontaneous ipsilateral flexor and extensor deletions. Specifically, during non-resetting flexor deletions the ipsilateral extensor root always showed sustained firing, whereas rhythmic flexor activity was never disturbed during non-resetting deletions of extensor activity. This may reflect a fundamental asymmetry in the organization of the neonatal mouse hindlimb locomotor CPG, which was previously suggested in studies of fictive and treadmill locomotion in cats (Pearson & Duysens, 1976, Duysens & Pearson, 1980; Whelan, 1996; Wilson *et al.* 2005; Duysens, 2006; Brownstone & Wilson, 2008). The adult decerebrate cat during MLR-evoked fictive locomotion exhibited more deletion types (Lafreniere-Roula & McCrea, 2005). Both flexor and extensor deletions could be accompanied by sustained activity in the antagonist nerves or muscles. However, while extensor deletions with unaffected flexor bursting were described in these and other cat locomotion studies, there were no clear examples in which flexor deletions were accompanied by unperturbed extensor bursting. This observation indirectly supports the so-called ‘flexor burst generator model’ originally suggested by Pearson & Duysens (1976), who hypothesized an asymmetric locomotor CPG in which a flexor rhythm generator is the dominant rhythm-generating half-centre (see also Duysens, 2006; Guertin, 2009). Our computational model combines the Rybak–McCrea concept of the two-level locomotor CPG (Rybak *et al.* 2006a,b; McCrea & Rybak, 2007, 2008) with the Duysens–Pearson concept of an asymmetric rhythm generator with a dominant flexor half-centre (Pearson & Duysens, 1976). Our experimental results are in full accordance with the Duysens–Pearson hypothesis, so in our current model, the RG layer includes only one intrinsically rhythmic half-centre which drives rhythmic flexor activity (the RG-F population). Based on the previous Rybak *et al.* (2006a) model, bursting in this population is based on a persistent (slowly inactivating) sodium current, present in all RG-F neurons, and mutual excitatory synaptic interactions within the RG-F population. The non-rhythmic extensor half-centre (the RG-E population) is tonically active. However, via inhibitory interactions with the intrinsically rhythmic flexor half-centre it can control the duration of the extensor phase, and the timing of switching to the next flexion. In addition, as we demonstrated in simulation (Fig. 11), excitatory interactions of this half-centre with

the contralateral RG-F, via specific excitatory CINs, may speed up locomotor oscillations; this can explain the experimentally observed slowing of the locomotor cycle frequency in the spinal cord after hemisection (Fig. 2A).

The proposed computational model was able to reproduce both types of non-resetting deletions observed in our experimental studies by inhibition of specific neuron classes in the model (Fig. 10). In addition, we used the model to simulate resetting perturbations and deletions (Fig. 12). These simulations emphasized that the important feature of resetting deletions (distinguishing them from non-resetting deletions) is the disturbance of rhythm and a corresponding post-deletion phase shift on both sides of the cord. Our model was able to reproduce the details of motoneuron activity during one experimental resetting deletion (compare Fig. 12B and C). In this connection, it is interesting to re-consider the exceptional deletion shown in Fig. 1D, when a flexor deletion in the ipsilateral flexor root (iL2) occurred simultaneously with an extensor deletion in the contralateral extensor (cL5) root. Because there was no phase shift after these deletions, they were formally classified as non-resetting. However, because rhythmic pattern disturbances were seen on both sides of the cord (which is typical of the resetting deletion type), it is possible that this episode represents a resetting deletion occurring with a zero phase shift. Note that the disturbances/deletions produced in this episode in all four ventral roots are qualitatively similar to those shown in Fig. 12C (though the sides of the cord are switched), which suggests that they are produced by qualitatively similar network perturbations such as those modelled in Fig. 12B. While the episode in Fig. 12C was resetting because it clearly exhibited a phase shift of locomotor oscillations after the deletions, this phase shift was insignificant in the episode shown in Fig. 1D. This suggests that deletion in Fig. 1D represents a 'degenerate case' of resetting deletions occurring with a zero phase shift.

Our model was built based on our experimental data of spontaneous deletions from the isolated neonatal mouse spinal cord preparation; it may not reflect CPG network organization in adult mice, or in more intact *in vivo* preparations. We believe that intrinsic properties of some CPG interneurons, and synaptic interactions between them, may change during postnatal maturation (for example see Abbinanti & Harris-Warrick, 2008; Husch *et al.* 2011), which could alter the function of the network as the animal gets older. Also, sensory feedback can affect the locomotor CPG at several levels (modelled by Rybak *et al.* 2006b; McCrea & Rybak, 2008) and modify their operation during real locomotion. Finally, deletions evoked by other means, such as pharmacological manipulation of synaptic strength (Talpalar & Kiehn, 2010), may affect network function in different ways from the spontaneous deletions we have studied, and provide additional insights into network organization.

Conclusion

The concept of a two-level CPG organization containing independently controlled rhythm-generating (RG) and pattern-forming (PF) networks was based on many lines of evidence (Perret & Cabelguen, 1980; Kriellaars *et al.* 1994; Guertin *et al.* 1995; Perreault *et al.* 1995; Rybak *et al.* 2006a,b; McCrea & Rybak, 2007, 2008). Our work in the neonatal mouse spinal cord confirms this earlier work, and, for the first time, provides electrophysiological recordings of identified interneurons (V2a and CINs) during non-resetting deletions predicted by the model for RG and PF neurons. These recordings have clearly demonstrated the flexor–extensor asymmetry in the neonatal mouse locomotor CPG. The challenge for the future is to place these interneurons more firmly in the network structure and show how they contribute to rhythmogenesis and locomotor pattern formation. Our model makes testable predictions of the synaptic drive that neurons at each point in the CPG should receive under control conditions and during different types of deletions; this should provide important information to assign functional roles to these and other identified interneurons.

Appendix

Modelling of single motoneurons and interneurons

In accordance with the two-compartment motoneuron model of Booth *et al.* (1997), but with the additional incorporation of the persistent sodium current (I_{NaP}) to the motoneuron dendrite, the membrane potentials of the motoneuron soma ($V_{(S)}$) and dendrite ($V_{(D)}$) are described by the following differential equations:

$$\begin{aligned} C \cdot \frac{dV_{(S)}}{dt} &= -I_{Na(S)} - I_{K(S)} - I_{CaN(S)} - I_{K,Ca(S)} \\ &\quad - I_{L(S)} - I_{C(S)}; \\ C \cdot \frac{dV_{(D)}}{dt} &= -I_{NaP(D)} - I_{CaN(D)} - I_{CaL(D)} - I_{K,Ca(D)} \\ &\quad - I_{L(D)} - I_{C(D)} - I_{SynE} - I_{SynI}, \quad (A1) \end{aligned}$$

where C is the membrane capacitance and t is time and indexes (S) and (D) indicate ionic currents in the soma and dendrite, respectively.

The dendrite–soma coupling currents (with conductance g_C) for soma $I_{C(S)}$ and dendrite $I_{C(D)}$ are described following the Booth *et al.* (1997) model:

$$\begin{aligned} I_{C(S)} &= \frac{g_C}{p} \cdot (V_{(S)} - V_{(D)}); \\ I_{C(D)} &= \frac{g_C}{1-p} \cdot (V_{(D)} - V_{(S)}), \quad (A2) \end{aligned}$$

Table 1. Maximal conductances of ionic channels and E_L in different neuron types

Neuron type	\bar{g}_{Na} (nS)	\bar{g}_{NaP} (nS)	\bar{g}_K (nS)	\bar{g}_{CaL} (nS)	\bar{g}_{CaN} (nS)	$\bar{g}_{K,Ca}$ (nS)	g_L (nS)	E_L^* (mV)
RG-F	30	0.35	2				0.09	-64 ± 0.64
RG-E	30	0.1	2				0.09	-60 ± 0.6
PF	30	0.1	2				0.09	-62 ± 0.62
All other interneurons	120		100				0.51	-64 ± 3.2
Mn soma	120		100		14	2	0.51	-68 ± 3.4
Mn dendrite		0.1		0.33	0.3	0.8	0.51	-68 ± 3.4

*To provide heterogeneity of neurons within neural populations, the value of E_L was randomly assigned from normal distributions (see mean values \pm SDs).

where p is the parameter defining the ratio of somatic surface area to total surface area.

The ionic currents in the model are described as follows:

$$\begin{aligned}
 I_{Na} &= \bar{g}_{Na} \cdot m_{Na}^3 \cdot h_{Na} \cdot (V - E_{Na}); \\
 I_{NaP} &= \bar{g}_{NaP} \cdot m_{NaP} \cdot h_{NaP} \cdot (V - E_{Na}); \\
 I_K &= \bar{g}_K \cdot m_K^4 \cdot (V - E_K); \\
 I_{CaN} &= \bar{g}_{CaN} \cdot m_{CaN}^2 \cdot h_{CaN} \cdot (V - E_{Ca}); \\
 I_{CaL} &= \bar{g}_{CaL} \cdot m_{CaL} \cdot (V - E_{Ca}); \\
 I_{K,Ca} &= \bar{g}_{K,Ca} \cdot m_{K,Ca} \cdot (V - E_K); \\
 I_L &= g_L \cdot (V - E_L),
 \end{aligned} \tag{A3}$$

where V is the membrane potential; I_{Na} is the fast sodium with maximal conductance \bar{g}_{Na} ; I_{NaP} is the persistent sodium current with maximal conductance \bar{g}_{NaP} ; I_K is the delayed-rectifier potassium current with maximal conductance \bar{g}_K ; I_{CaN} is the N-type calcium current with maximal conductance \bar{g}_{CaN} ; I_{CaL} is the L-type calcium current with maximal conductance \bar{g}_{CaL} ; $I_{K,Ca}$ is calcium-dependent potassium current with maximal conductance $\bar{g}_{K,Ca}$; I_L is the leakage current with conductance g_L ; E_{Na} , E_K , E_{Ca} , and E_L are the reversal potentials for sodium, potassium, calcium and leakage current, respectively.

For simplicity and because of the lack of specific data, all interneurons (single-compartment models) except RG and PF neurons contain only a minimal set of ionic currents:

$$C \cdot \frac{dV}{dt} = -I_{Na} - I_K - I_L - I_{SynE} - I_{SynI}. \tag{A4}$$

The excitatory neurons of the CPG comprising the RG and PF populations have the persistent (slowly inactivating) sodium current, I_{NaP} :

$$C \cdot \frac{dV}{dt} = -I_{Na} - I_{NaP} - I_K - I_L - I_{SynE} - I_{SynI}. \tag{A5}$$

However, only RG-F neurons have maximal conductance of this current (\bar{g}_{NaP}) large enough to activate endogenous bursting properties in these neurons.

Maximal conductances of all ionic currents for all neuron types are listed in Table 1.

Activation m and inactivation h of voltage-dependent ionic channels (e.g. Na^+ , NaP^+ , K^+ , Ca_N^{2+} , Ca_L^{2+}) are described by the following differential equations:

$$\begin{aligned}
 \tau_{mi}(V) \cdot \frac{d}{dt} m_i &= m_{\infty i}(V) - m_i; \\
 \tau_{hi}(V) \cdot \frac{d}{dt} h_i &= h_{\infty i}(V) - h_i,
 \end{aligned} \tag{A6}$$

where i identifies the name of the channel, $m_{\infty i}(V)$ and $h_{\infty i}(V)$ define the voltage-dependent steady-state activation and inactivation, respectively, and $\tau_{mi}(V)$ and $\tau_{hi}(V)$ define the corresponding time constants. Activation of the sodium channels is considered to be instantaneous ($\tau_{mNa} = \tau_{mNaP} = 0$). The parameters and expression for all channel kinetics can be found in Table 2.

The kinetics of intracellular Ca^{2+} concentration (Ca, described separately for each compartment) is modelled according to the following equation (Booth *et al.* 1997):

$$\frac{d}{dt} Ca = f \cdot (-\alpha \cdot I_{Ca} - k_{Ca} \cdot Ca), \tag{A7}$$

where f defines the percentage of free to total Ca^{2+} ; α converts the total Ca^{2+} current, I_{Ca} , to Ca^{2+} concentration; k_{Ca} represents the Ca^{2+} removal rate.

Activation of the Ca^{2+} -dependent potassium channels is considered instantaneous and described as follows (Booth *et al.* 1997):

$$m_{K,Ca} = \frac{Ca}{Ca + K_d}, \tag{A8}$$

where Ca is the Ca^{2+} concentration within the corresponding compartment or neurone, and K_d defines the half-saturation level of this conductance.

Synaptic excitatory (I_{SynE} with conductance g_{SynE} and reversal potential E_{SynE}) and inhibitory (I_{SynI} with conductance g_{SynI} and reversal potential E_{SynI}) currents have also been incorporated into our models:

$$\begin{aligned}
 I_{SynE} &= g_{SynE} \cdot (V - E_{SynE}); \\
 I_{SynI} &= g_{SynI} \cdot (V - E_{SynI}).
 \end{aligned} \tag{A9}$$

Table 2. Steady state activation and inactivation variables and time constants for voltage-dependent ionic channels

Ionic channels	$m_{\infty}(V)$; V is in mV $h_{\infty}(V)$; V is in mV	$\tau_m(V)$ (ms) $\tau_h(V)$ (ms)
Na ⁺	$m_{\infty\text{Na}} = (1 + \exp(-(V + 35)/7.8))^{-1}$ $h_{\infty\text{Na}} = (1 + \exp((V + 55)/7))^{-1}$	$\tau_{m\text{Na}} = 0$ $\tau_{h\text{Na}} = 30/(\exp((V + 50)/15) + \exp(-(V + 50)/16))$
Na _P ⁺	$m_{\infty\text{NaP}} = (1 + \exp(-(V + 47.1)/3.1))^{-1}$ $h_{\infty\text{NaP}} = (1 + \exp((V + 59)/10))^{-1}$	$\tau_{m\text{NaP}} = 0$ $\tau_{h\text{NaP}} = \tau_{h\text{NaPmax}}/\cosh(V + 59)/20$, $\tau_{h\text{NaPmax}} = 10000$
K ⁺	$m_{\infty\text{K}} = (1 + \exp(-(V + 28)/15))^{-1}$ $h_{\text{K}} = 1$	$\tau_{m\text{K}} = 7/(\exp((V + 40)/40) + \exp(-(V + 40)/50))$
Ca _N ²⁺	$m_{\infty\text{CaN}} = (1 + \exp(-(V + 30)/5))^{-1}$ $h_{\infty\text{CaN}} = (1 + \exp((V + 45)/5))^{-1}$	$\tau_{m\text{CaN}} = 4$ $\tau_{h\text{CaN}} = 40$
Ca _L ²⁺	$m_{\infty\text{CaL}} = (1 + \exp(-(V + 40)/7))^{-1}$ $h_{\text{CaL}} = 1$	$\tau_{m\text{CaL}} = 40$

All expressions and parameters, except for Na_P⁺, are taken from Booth *et al.* (1997). The expressions for the Na_P⁺ channel are from Rybak *et al.* (2003).

The excitatory (g_{SynE}) and inhibitory synaptic (g_{SynI}) conductances are equal to zero at rest and may be activated (opened) by the excitatory or inhibitory inputs respectively:

$$\begin{aligned}
 g_{\text{SynE}i}(t) &= \bar{g}_{\text{E}} \cdot \sum_j S\{w_{ji}\} \cdot \sum_{t_{kj} < t} \exp(-(t - t_{kj})/\tau_{\text{SynE}}) \\
 &\quad + \bar{g}_{\text{Ed}} \cdot \sum_m S\{w_{dmi}\} \cdot d_{mi}; \\
 g_{\text{SynI}i}(t) &= \bar{g}_{\text{I}} \cdot \sum_j S\{-w_{ji}\} \cdot \sum_{t_{kj} < t} \exp(-(t - t_{kj})/\tau_{\text{SynI}}) \\
 &\quad + \bar{g}_{\text{Id}} \cdot \sum_m S\{-w_{dmi}\} \cdot d_{mi}, \quad (\text{A10})
 \end{aligned}$$

where the function $S\{x\} = x$, if $x \geq 0$, and 0 if $x < 0$.

According to eqn (A10), the excitatory and inhibitory synaptic conductances have two terms. The first term describes the integrated effect of inputs from other neurones in the network (excitatory and inhibitory respectively). The second term describes the effect of external drives used to simulate applied perturbations. Each spike arriving to neurone i from neurone j at time t_{kj} increases the excitatory synaptic conductance by $\bar{g}_{\text{E}} \cdot w_{ji}$ if the synaptic weight $w_{ji} > 0$, or increases the inhibitory synaptic conductance by $-\bar{g}_{\text{I}} \cdot w_{ji}$ if the synaptic weight $w_{ji} < 0$. \bar{g}_{E} and \bar{g}_{I} are the parameters defining an increase in the excitatory or inhibitory synaptic conductance, respectively, produced by one arriving spike at $|w_{ji}| = 1$. τ_{SynE} and τ_{SynI} are the decay time constants for the excitatory and inhibitory conductances, respectively. In the second terms of eqn (A10), \bar{g}_{Ed} and \bar{g}_{Id} are the parameters defining the increase in the excitatory or inhibitory synaptic conductance, respectively, produced by external input drive $d_{mi} = 1$ with a synaptic weight of $|w_{dmi}| = 1$. The weights of all synaptic connections between the neural populations are shown in Table 3.

Table 3. Weights of synaptic connections in the network

Target population*	Source population or drive (weight of synaptic input to one neuron)
i-CINe-F	i-RG-F (0.015)
i-CINi-F	i-RG-F (0.015)
i-CINe-E	i-RG-E (0.03)
i-RG-F	i-RG-F (0.0025) with probability 0.1; i-ln-RG-E (0.002); c-CINe-F (0.00006); c-CINi-F (-0.012); c-CINe-E (0.005)
i-RG-E	i-RG-E (0.005); c-CINe-F (0.01)
i-ln-RG-F	i-RG-F (0.015)
i-ln-RG-E	i-RG-E (0.015); i-ln-RG-F (-0.6)
i-PF-F	i-RG-F (0.003); i-ln-PF-F (-0.0025)
i-PF-E	i-RG-E (0.018); i-ln-PF-E (-0.13)
i-ln-PF-F	i-PF-E (0.04); i-ln-PF-E (-0.013)
i-ln-PF-E	i-PF-F (0.04); i-ln-PF-F (-0.013)
i-la-F	i-PF-F (0.06); i-la-E (-0.04); i-R-F (-0.04)
i-la-E	i-PF-E (0.06); i-la-F (-0.04); i-R-E (-0.04)
i-R-F	i-Mn-F (0.1); i-R-E (-0.02)
i-R-E	i-Mn-E (0.1); i-R-F (-0.02)
i-Mn-F	i-PF-F (0.035); i-la-E (-0.1); i-R-F (-0.04)
i-Mn-E	i-PF-E (0.035); i-la-F (-0.1); i-R-E (-0.04)

*Prefixes i- and c- indicate ipsi- and contralateral populations. Values in brackets represent relative weights of synaptic inputs from the corresponding source populations (w_{ji}).

Other neuronal parameters. General parameters: $E_{\text{Na}} = 55$ mV; $E_{\text{K}} = -80$ mV; $E_{\text{Ca}} = 80$ mV; $C = 1$ $\mu\text{F cm}^{-2}$; $g_{\text{C}} = 0.1$ mS/cm²; $p = 0.1$; $f = 0.01$; $\alpha = 0.0009$ mol C⁻¹ μm^{-1} ; $k_{\text{Ca}} = 2$ ms⁻¹; $K_{\text{d}} = 0.2$ μM .

Parameters of synapses: $E_{\text{SynE}} = -10$ mV; $E_{\text{SynI}} = -70$ mV; $\bar{g}_{\text{E}} = 0.05$ mS cm⁻²; $\bar{g}_{\text{I}} = 0.05$ mS cm⁻²; $\bar{g}_{\text{Ed}} = 0.05$ mS cm⁻²; $\bar{g}_{\text{Id}} = 0.05$ mS cm⁻²; $\tau_{\text{SynE}} = 5$ ms; $\tau_{\text{SynI}} = 5$ ms.

Modelling neural populations

Each type of neuron in the model was represented by a population of neurons. In all simulations in this paper, RG-F population consisted of 200 neurons, RG-E, PF-F, PF-E and both MN populations consisted of 100 neurons, and all other populations contained 50 neurons. Connections between populations were established such that if a population A was assigned to receive an excitatory or inhibitory input from a population B or external drive D, then each neurone in the population A received the corresponding excitatory or inhibitory synaptic input from each neuron in the population B or from drive D with a probability of connection P_{AB} or P_{AD} , respectively (a random generator was used to define the existence of each connection if P_{AB} or P_{AD} was not equal to 1). For all interconnections between populations, except for those inside the left and right RG-F (l-RG-F and r-RG-F) these probabilities were set to 1. For mutual interconnections within l-RG-F and r-RG-F populations, the probabilities of connections were set to 0.1. Heterogeneity of neurons within each population was set by a random distribution of leak reversal potential E_L in each neuron and initial conditions for all slow variables. The latter were chosen randomly from a uniform distribution for each variable, and a settling period of 50 s was allowed in each simulation before data were collected. Each simulation was repeated 10–15 times, and demonstrated qualitatively similar behaviour for particular values of the standard deviation of E_L and initial conditions.

References

- Abbinanti MD & Harris-Warrick RM (2008). Postnatal development of firing properties and serotonergic modulation of commissural interneurons in the mouse spinal cord. *2008 Abstract Viewer/Itinerary Planner*, Programme No. 373.6. Society for Neuroscience, Washington, DC.
- Al-Mosawie A, Wilson JM & Brownstone RM (2007). Heterogeneity of V2-derived interneurons in the adult mouse spinal cord. *Eur J Neurosci* **26**, 3003–3015.
- Booth V, Rinzel J & Kiehn O (1997). Compartmental model of vertebrate motoneurons for Ca^{2+} -dependent spiking and plateau potentials under pharmacological treatment. *J Neurophysiol* **78**, 3371–3385.
- Bonnot A, Whelan PJ, Mentis GZ & O'Donovan MJ (2002). Spatiotemporal pattern of motoneuron activation in the rostral lumbar and the sacral segments during locomotor-like activity in the neonatal mouse spinal cord. *J Neurosci* **22**, RC203.
- Brocard F, Tazerart S & Vinay L (2010). Do pacemakers drive the central pattern generator for locomotion in mammals? *Neuroscientist* **16**, 139–155.
- Brownstone RM & Wilson JM (2008). Strategies for delineating spinal locomotor rhythm-generating networks and the possible role of Hb9 interneurons in rhythmogenesis. *Brain Res Rev* **57**, 64–76.
- Butt SJ, Harris-Warrick RM & Kiehn O (2002). Firing properties of identified interneuron populations in the mammalian hindlimb central pattern generator. *J Neurosci* **22**, 9961–9971.
- Butt SJ & Kiehn O (2003). Functional identification of interneurons responsible for left–right coordination of hindlimbs in mammals. *Neuron* **38**, 953–963.
- Butt SJ, Lundfald L & Kiehn O (2005). EphA4 defines a class of excitatory locomotor-related interneurons. *Proc Natl Acad Sci U S A* **102**, 14098–14103.
- Cazalets JR, Borde M & Clarac F (1995). Localization and organization of the central pattern generator for hindlimb locomotion in newborn rat. *J Neurosci* **15**, 4943–4951.
- Cowley KC & Schmidt BJ (1995). Effects of inhibitory amino acid antagonists on reciprocal inhibitory interactions during rhythmic motor activity in the in vitro neonatal rat spinal cord. *J Neurophysiol* **74**, 1109–1117.
- Cowley KC & Schmidt BJ (1997). Regional distribution of the locomotor pattern-generating network in the neonatal rat spinal cord. *J Neurophysiol* **77**, 247–259.
- Crone SA, Quinlan KA, Zagoraïou L, Droho S, Restrepo CE, Lundfald L, Endo T, Setlak J, Jessell TM, Kiehn O & Sharma K (2008). Genetic ablation of V2a ipsilateral interneurons disrupts left–right locomotor coordination in mammalian spinal cord. *Neuron* **60**, 70–83.
- Crone SA, Zhong G, Harris-Warrick R & Sharma K (2009). In mice lacking V2a interneurons, gait depends on speed of locomotion. *J Neurosci* **29**, 7098–7109.
- Dougherty KJ & Kiehn O (2010). Firing and cellular properties of V2a interneurons in the rodent spinal cord. *J Neurosci* **30**, 24–37.
- Duysens J (1977). Reflex control locomotion as revealed by stimulation of cutaneous afferents in spontaneously walking pre-mammillary cats. *J Neurophysiol* **40**, 737–751.
- Duysens J & Pearson KG (1980). Inhibition of flexor burst generator by loading ankle extensor muscles in walking cats. *Brain Res* **187**, 321–332.
- Duysens J (2006). How deletions in a model could help explain deletions in the laboratory. *J Neurophysiol* **95**, 562–563.
- Falgairolle M & Cazalets JR (2007). Metachronal coupling between spinal neuronal networks during locomotor activity in newborn rat. *J Physiol* **580**, 87–102.
- Gosgnach S, Lanuza GM, Butt SJ, Saueressig H, Zhang Y, Velasquez T, Riethmacher D, Callaway EM, Kiehn O & Goulding M (2006). V1 spinal neurons regulate the speed of vertebrate locomotor outputs. *Nature* **440**, 215–219.
- Goulding M (2009). Circuits controlling vertebrate locomotion: moving in a new direction. *Nat Rev Neurosci* **10**, 507–518.
- Geertsens SS, Stecina K, Meehan CF, Nielsen JB & Hultborn H (2011). Reciprocal Ia inhibition contributes to motoneuronal hyperpolarisation during the inactive phase of locomotion and scratching in the cat. *J Physiol* **589**, 119–134.
- Graham-Brown T (1911). The intrinsic factors in the act of progression in mammals. *Proc R Soc B* **84**, 308–319.

- Grillner S (1981). Control of locomotion in bipeds, tetrapods, and fish. In *Handbook of Physiology*, section 1, *The Nervous System*, vol. II, *Motor Control*, ed. Brooks VB, pp. 1179–1236. American Physiology Society, Bethesda, MD.
- Grillner S (2006). Biological pattern generation: the cellular and computational logic of networks in motion. *Neuron* **52**, 751–766.
- Grillner S & Zangger P (1979). On the central generation of locomotion in the low spinal cat. *Exp Brain Res* **34**, 241–261.
- Guertin PA (2009). The mammalian central pattern generator for locomotion. *Brain Res Rev* **62**, 45–56.
- Guertin P, Angel MJ, Perreault MC & McCrea DA (1995). Ankle extensor group I afferents excite extensors throughout the hindlimb during fictive locomotion in the cat. *J Physiol* **487**, 197–209.
- Hanson MG & Landmesser LT (2003). Characterization of the circuits that generate spontaneous episodes of activity in the early embryonic mouse spinal cord. *J Neurosci* **23**, 587–600.
- Hinckley CA, Hartley R, Wu L, Todd A & Ziskind-Conhaim L (2005). Locomotor-like rhythms in a genetically distinct cluster of interneurons in the mammalian spinal cord. *J Neurophysiol* **93**, 1439–1449.
- Husch A, Cramer N & Harris-Warrick RM (2011). Long-duration perforated patch recordings from spinal interneurons of adult mice. *J Neurophysiol* **106**, 2783–2789.
- Jankowska E (1992). Interneuronal relay in spinal pathways from proprioceptors. *Prog Neurobiol* **38**, 335–378.
- Jankowska E, Hammar I, Slawinska U, Maleszak K & Edgley SA (2003). Neuronal basis of crossed actions from the reticular formation on feline hindlimb motoneurons. *J Neurosci* **23**, 1867–1878.
- Jankowska E, Krutki P & Matsuyama K (2005). Relative contribution of Ia inhibitory interneurons to inhibition of feline contralateral motoneurons evoked via commissural interneurons. *J Physiol* **568**, 617–628.
- Jankowska E (2008). Spinal interneuronal networks in the cat: elementary components. *Brain Res Rev* **57**, 46–55.
- Kiehn O (2006). Locomotor circuits in the mammalian spinal cord. *Annu Rev Neurosci* **29**, 279–306.
- Kiehn O & Kjaerulff O (1998). Distribution of central pattern generators for rhythmic motor outputs in the spinal cord of limbed vertebrates. *Ann NY Acad Sci* **860**, 110–129.
- Kjaerulff O & Kiehn O (1996). Distribution of networks generating and coordinating locomotor activity in the neonatal rat spinal cord in vitro: a lesion study. *J Neurosci* **16**, 5777–5794.
- Kriellaars DJ, Brownstone RM, Noga BR & Jordan LM (1994). Mechanical entrainment of fictive locomotion in the decerebrate cat. *J Neurophysiol* **71**, 2074–2086.
- Kwan AC, Dietz SB, Webb WW & Harris-Warrick RM (2009). Activity of Hb9 interneurons during fictive locomotion in mouse spinal cord. *J Neurosci* **29**, 11601–11613.
- Lafreniere-Roula M & McCrea DA (2005). Deletions of rhythmic motoneuron activity during fictive locomotion and scratch provide clues to the organization of the mammalian central pattern generator. *J Neurophysiol* **94**, 1120–1132.
- Lanuza GM, Gosgnach S, Pierani A, Jessell TM & Goulding M (2004). Genetic identification of spinal interneurons that coordinate left-right locomotor activity necessary for walking movements. *Neuron* **42**, 375–386.
- Lundberg A (1981). Half-centres revisited. In *Regulatory Functions of the CNS. Motion and Organization Principles*, ed. Szentagothai J, Palkovits M & Hamori J, pp. 155–167. Pergamon Akademi Kiado, Budapest.
- Lundfald L, Restrepo CE, Butt SJ, Peng CY, Droho S, Endo T, Zeilhofer HU, Sharma K & Kiehn O (2007). Phenotype of V2-derived interneurons and their relationship to the axon guidance molecule EphA4 in the developing mouse spinal cord. *Eur J Neurosci* **26**, 2989–3002.
- McCrea DA, Pratt CA & Jordan LM (1980). Renshaw cell activity and recurrent effects on motoneurons during fictive locomotion. *J Neurophysiol* **44**, 475–488.
- McCrea DA & Rybak IA (2007). Modeling the mammalian locomotor CPG: insights from mistakes and perturbations. *Prog Brain Res* **165**, 235–253.
- McCrea DA & Rybak IA (2008). Organization of mammalian locomotor rhythm and pattern generation. *Brain Res Rev* **57**, 134–146.
- Pearson KG & Duysens J (1976). Function of segmental reflexes in the control of stepping in cockroaches and cats. In *Neural Control of Locomotion*, ed. Herman RM, Grillner S, Stein PSG, and Stuart DG, pp. 519–537. Plenum Press, New York.
- Perreault MC, Angel MJ, Guertin P & McCrea DA (1995). Effects of stimulation of hindlimb flexor group II afferents during fictive locomotion in the cat. *J Physiol* **487**, 211–220.
- Perret C & Cabelguen JM (1980). Main characteristics of the hindlimb locomotor cycle in the decorticate cat with special reference to bifunctional muscles. *Brain Res* **18**, 333–352.
- Pratt CA & Jordan LM (1987). Ia inhibitory interneurons and Renshaw cells as contributors to the spinal mechanisms of fictive locomotion. *J Neurophysiol* **57**, 56–71.
- Quinlan KA & Kiehn O (2007). Segmental, synaptic actions of commissural interneurons in the mouse spinal cord. *J Neurosci* **27**, 6521–6530.
- Rybak IA, Shevtsova NA, Lafreniere-Roula M & McCrea DA (2006a). Modelling spinal circuitry involved in locomotor pattern generation: insights from deletions during fictive locomotion. *J Physiol* **577**, 617–639.
- Rybak IA, Shevtsova NA, St.-John WM, Paton JFR & Pierrefiche O (2003). Endogenous rhythm generation in the pre-Böttinger Complex and ionic currents: Modelling and in vitro studies. *Eur J Neurosci* **18**, 239–257.
- Rybak IA, Stecina K, Shevtsova NA & McCrea DA (2006b). Modelling spinal circuitry involved in locomotor pattern generation: insights from the effects of afferent stimulation. *J Physiol* **577**, 641–658.
- Shefchyk S & Jordan LM (1985). Excitatory and inhibitory post-synaptic potentials in α -motoneurons produced during fictive locomotion by stimulation of the mesencephalic locomotor region. *J Neurophysiol* **53**, 1345–1355.
- Stein PS & Daniels-McQueen S (2002). Modular organization of turtle spinal interneurons during normal and deletion fictive rostral scratching. *J Neurosci* **22**, 6800–6809.
- Stein PS & Daniels-McQueen S (2004). Variations in motor patterns during fictive rostral scratching in the turtle: knee-related deletions. *J Neurophysiol* **91**, 2380–2384.

- Stein PS (2008). Motor pattern deletions and modular organization of turtle spinal cord. *Brain Res Rev* **57**, 118–124.
- Talpalar AE & Kiehn O (2010). Glutamatergic mechanisms for speed control and network operation in the rodent locomotor CPG. *Frontiers Neural Networks* **4**, pii, 19.
- Tazerart S, Vinay L & Brocard F (2008). The persistent sodium current generates pacemaker activities in the central pattern generator for locomotion and regulates the locomotor rhythm. *J Neurosci* **28**, 8577–8589.
- Whelan PJ (1996). Control of locomotion in the decerebrate cat. *Prog Neurobiol* **49**, 481–515.
- Wilson JW, Hartley R, Maxwell DJ, Todd AJ, Lieberam I, Kaltschmidt JA, Yoshida Y, Jessell TM & Brownstone RM (2005). Conditional rhythmicity of ventral spinal interneurons defined by expression of the Hb9 homeodomain protein. *J Neurosci* **25**, 5710–5719.
- Zagoraoui L, Akay T, Martin JF, Brownstone RM, Jessell TM & Miles GB (2009). A cluster of cholinergic premotor interneurons modulates mouse locomotor activity. *Neuron* **64**, 645–662.
- Zaporozhets E, Cowley KC & Schmidt BJ (2004). A reliable technique for the induction of locomotor-like activity in the in vitro neonatal rat spinal cord using brainstem electrical stimulation. *J Neurosci Methods* **139**, 33–41.
- Zhang Y, Narayan S, Geiman E, Lanuza GM, Velasquez T, Shanks B, Akay T, Dyck J, Pearson K, Gosgnach S, Fan CM & Goulding M (2008). V3 spinal neurons establish a robust and balanced locomotor rhythm during walking. *Neuron* **60**, 84–96.
- Zhong G, Diaz-Rios ME & Harris-Warrick RM (2006a). Serotonin modulates the properties of ascending commissural interneurons in the neonatal mouse spinal cord. *J Neurophysiol* **95**, 1545–1555.
- Zhong G, Diaz-Rios M & Harris-Warrick RM (2006b). Intrinsic and functional differences among commissural interneurons during fictive locomotion and serotonergic modulation in the neonatal mouse. *J Neurosci* **26**, 6509–6517.
- Zhong G, Droho S, Crone SA, Dietz S, Kwan AC, Webb WW, Sharma K & Harris-Warrick RM (2010). Electrophysiological characterization of V2a interneurons and their locomotor-related activity in the neonatal mouse spinal cord. *J Neurosci* **30**, 170–182.
- Zhong G, Masino MA & Harris-Warrick RM (2007). Persistent sodium currents participate in fictive locomotion generation in neonatal mouse spinal cord. *J Neurosci* **27**, 4507–4518.
- Zhong G, Sharma K & Harris-Warrick RM (2011). Frequency-dependent recruitment of V2a interneurons during fictive locomotion in the mouse spinal cord. *Nat Commun* **2**, 274.
- Ziskind-Conhaim L, Mentis GZ, Wiesner EP & Titus JP (2010). Synaptic integration of rhythmogenic neurons in the locomotor circuitry: the case of Hb9 interneurons. *Ann N Y Acad Sci* **1198**, 72–84.

Author contributions

The experiments in this study were performed in the Department of Neurobiology and Behaviour, Cornell University, and the modelling and simulations were performed in the Department of Neurobiology and Anatomy, Drexel University. G.Z. and R.H.W. conceived and designed the electrophysiological experiments. G.Z. collected and analysed the experimental data. N.S. and I.R. developed the model and conducted all simulations. G.Z., N.S., I.R. and R.H.W. drafted and revised the article. All authors approved the final version for publication.

Acknowledgements

We thank Bruce Johnson, Andreas Husch and Shelby Dietz for important conversations and input to this manuscript, and Vinay Patel and Connor Benton for assistance in data analysis. This work was supported by NIH grants NS17323 and NS057599, and NSF grant IOS-0749467 to R. Harris-Warrick, and NIH grant NS04884 to I. Rybak.

Author's present address

G. Zhong: Department of Chemistry and Chemical Biology, Harvard University, Cambridge, MA, USA.